Spring 2017

CFD validation and scaling of condensation heat transfer

Varun Kalra

CFD VALIDATION AND SCALING OF CONDENSATION HEAT TRANSFER

by

VARUN KALRA

A THESIS

Presented to the Graduate Faculty of the

MISSOURI UNIVERSITY OF SCIENCE AND TECHNOLOGY

In Partial Fulfillment of the Requirements for the Degree

MASTER OF SCIENCE IN NUCLEAR ENGINEERING

2017

Approved by

Joshua Schlegel, Advisor
Shoaib Usman
Ayodeji B. Alajo

ABSTRACT

A CFD study was performed using STAR-CCM+ to validate the software for its competence in the prediction and scaling of condensation heat transfer in the presence of air acting as a non-condensable gas. Three vertical concentric tube heat exchanger geometries with different diameters were studied in the CFD analysis. It was seen that the steam bulk temperatures predicted by STAR-CCM+ closely matched the experimental data. However, the temperatures of outer wall of the steel condenser tubes showed a deviation of 2% to 11% from the experimental values. The error in adiabatic water wall temperatures were found to range from 18% to 6%. In general, the errors were larger closer to the steam inlet and reduced gradually towards the downstream regions. The error in heat transfer coefficients was much larger, with a maximum of 67.8% near the steam inlet. A scaling analysis was performed to study the ability of the software to predict the heat transfer coefficients for different diameter pipes. Although the software predicted that the heat transfer coefficient will reduce with increased diameter, the predictions failed to produce acceptable results. It was concluded that a further improvement is needed to the inbuilt software code for providing better predictions. Additional experiments are required to provide a basis for modifying the inbuilt correlations to provide an acceptable scaling analysis.

ACKNOWLEDGMENTS

I would like to express my gratitude to my advisor Dr. Joshua Schlegel for his unconditional support and motivation throughout the period of my graduate studies. I would like to thank him for teaching me how to excel in the academic, personal and professional fronts of my life. Further, I would like to thank him along with the Department of Nuclear Engineering for funding my studies and research at Missouri University of Science and Technology.

I would like to extend my gratitude to my committee members Dr. Shoaib Usman and Dr. Ayodeji B. Alajo for their valuable suggestions and thorough guidance that helped me in proper planning and execution of my thesis. I would also like to thank the Small Modular Reactor Research and Education Consortium, specifically the director, Dr. Joseph Smith, as well as Frieda Adams. Their support and assistance with research space and administration has been essential to the completion of this project.

Finally, I would like to thank my friends and family members for their constructive criticism and financial and moral support that has guided me to the successful completion of my graduate studies at Missouri University of Science and Technology.

TABLE OF CONTENTS

LIST OF FIGURES

Page

LIST OF TABLES

Page

NOMENCLATURE

Acronyms

SMR	Small Modular Reactor
PCCS	Passive containment cooling system
CNV	Containment vessel
LOCA	Loss of Coolant Accident
NRC	Nuclear Regulatory Commission
HTC	Heat Transfer Coefficient
NPT	National Pipe Thread taper
PWR	Pressurized Water Reactor

Latin Characters

D	Diameter [m]
T	Temperature [K]
A	Area [m^2]
M	Mass [kg]
U	Overall heat transfer coefficient [W/m^2K]
q	Total Heat [W]
Nu	Nusselt number
m''	Condensation mass flux

Greek

δ	Film thickness
β_f	Momentum transfer blowing parameter
Γ	Liquid flow per unit perimeter
μ	Dynamic viscosity
τ_i	Interfacial shear stress
ρ	Density

1. INTRODUCTION

1.1. BACKGROUND

26th June 1954 is marked as the day in history at which the world's first commercial reactor started feeding power to the electrical grid in the town of Obninsk, USSR. [1] Since then, the total number of nuclear power reactors in operation has increased to 442 as of December 2015. Combined, they account to a net installed capacity of 382451 (MWe) of nuclear power throughout the world. [2] Countries today have a predilection to add nuclear power to their portfolio of energy supply for various reasons. These reasons range from socioeconomic development to energy security and environmental considerations like reducing the global warming caused by accumulation of greenhouse gases. [3]

Although today one can see a definite increase of world nuclear power since its inception, the growth is not a linear one. Over the decades, the expansion of nuclear power has experienced some fluctuation due to various reasons. In 1973, the oil crisis raised concerns about oil supply security amongst major oil importers. This prompted many countries which were a member of the Organization for Economic Co-operation and Development (OECD) to create policies which shifted their dependence from oil power to nuclear power. [4] This boom went on to increase the share of nuclear power in the world electricity generation industry to 17% by the latter half of 1980s. This growth was hampered by the accidents of Three Mile Island and Chernobyl. This lead to a decrease of world nuclear share to 12% in early 2010. [3]

Accidents like these along with the recent Fukushima accident of March 11, 2011 have raised some safety concerns in not just the scientific community but among the public and political community as well. This, together with global financial and greenhouse gas concerns has resulted in the emergence of a new breed of nuclear reactors recognized as Small Modular Reactors (SMRs).

1.2. SMALL MODULAR REACTORS

The economy of scale, leading to larger, more efficient, higher output reactor systems, has dominated the nuclear industry for decades. Recently the development of

SMRs has come to the fore to address concerns over initial capital cost, safety, financing, and proliferation concerns. As the name suggests, SMRs are small and compact by design. These reactors are rated for an energy output of 300MWe or less, as opposed to state of the art reactors which produce 1000MWe or more. [5]

SMRs enjoy various benefits unavailable to the contemporary reactors. These include the capability of off-site fabrication, lower capital cost, enhanced passive safety and operational flexibility. SMRs also support a modular construction as more than one unit can be integrated to make a larger system in the same complex. Such systems can undergo scheduled maintenance independent of each other. This helps in maximizing profits by increasing the overall availability factor of the complex.

The major challenges faced by SMRs today include a lack of safety analysis studies, which can help in licensing and approval of upcoming SMR designs. Another major challenge is that the operational costs are higher based on the current policies for operators required to run a reactor. However, further research can help with the ease of licensing and policy changes can facilitate lower operational costs by allowing for less number of operators per reactor.

1.2.1. Westinghouse SMR. The W-SMR safety system design is passive and is based on the design of Westinghouse AP1000 reactor. It provides reduction in the effect of postulated accidents without the need of external intervention for seven days after an accident. The integral design as seen by Figure 1.1, results in the elimination of large piping loops which decreases the probability of loss of coolant accidents (LOCAs). The containment vessel (CV) of the W-SMR is a compact and high pressure design. The CV is submerged in a pool of water called the Outside Containment Pool (OCP). This aids the heat removal process in case of a postulated LOCA. [6] The effect of infrequent faults like LOCAs are reduced by injection of large quantities of water from the in-containment pool and the core makeup tank into the reactor vessel. An automatic depressurization system (ADS) is used to reduce the pressure of reactor vessel by venting steam into the containment to enable passive injection. The long-term decay heat removal system includes a Passive Containment Cooling System (PCCS) which operates by heat transfer through the CV wall to the surroundings. [6]

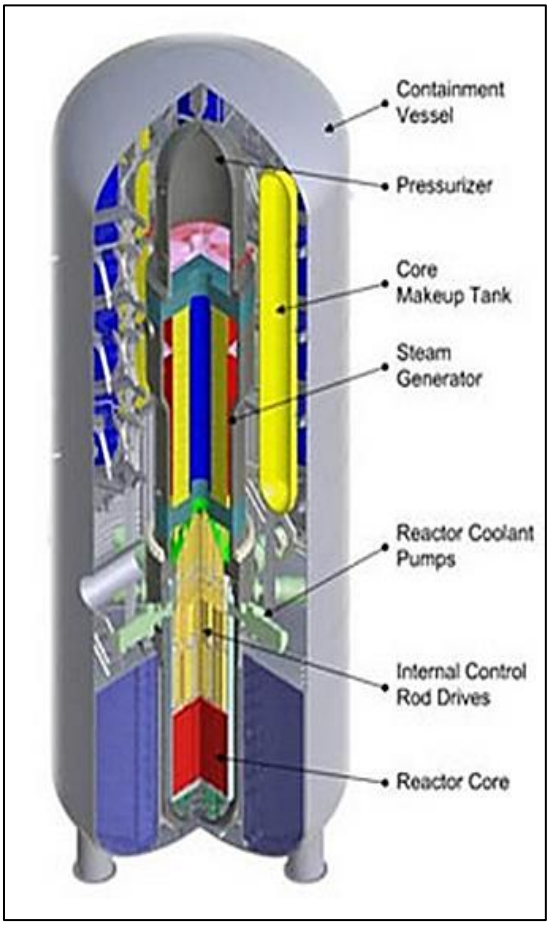

Figure 1.1 W-SMR [7]

1.2.2. Nuscale SMR. The NuScale SMR shown in Figure 1.2 is another example of an integral PWR. It is a light water reactor based on natural circulation with the reactor core and a helical steam generator located within the Reactor Vessel (RV). The RV is encapsulated in a cylindrical steel containment. The maximum output for this SMR is rated at 160MWt (45MWe). [7] Several key safety features of this SMR are detailed in Table 1.1. This reactor also operates in an evacuated containment and vents steam into the containment in the event of an accident. Like the W-SMR it is submerged to promote heat transfer out of the containment during an accident.

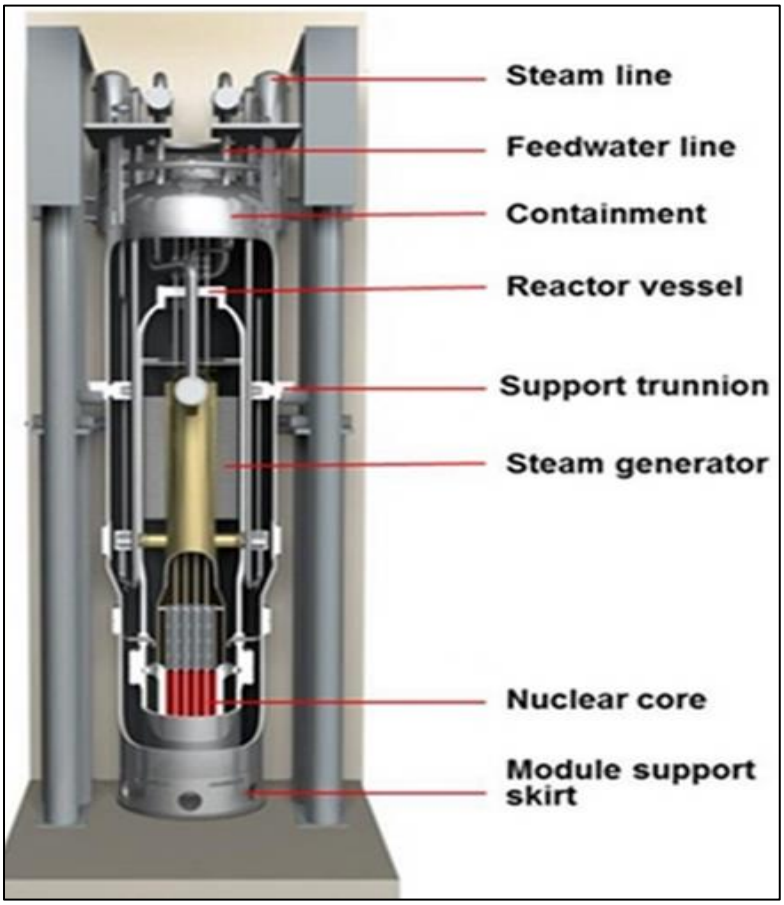

Figure 1.2 Nuscale SMR [8]

Table 1.1 Nuscale SMR design features and safety impacts [8]

Nuscale Design Feature	Primary Impact	Safety
RPV Integral reactor cooling system	Absence of large diameter piping for primary coolant	LOCA accidents are eliminated
Core cooled by natural convection	Absence of reactor coolant pumps	Accident of reactor coolant pump, pump seizure, shafts breaks, pump leaks and missile generation are eliminated
High pressure containment design	Equilibrium CNV pressure remains below containment design pressure for the worst design based accident.	Assured containment Integrity.

Table 1.1 Nuscale SMR design features and safety impacts [8] (cont.)

Modular NSSS and reactor vessel inside the CNV	Any water lost from reactor vessel does not leave the containment.	Nuclear fuel remains covered due to absence of postulated LOCA on design basis.
Evacuated containment	Lower than atmospheric pressure during normal operation	Higher containment cooling for steam condensation during a postulated small-break LOCA.
	No insulation on reactor vessel	Ex-vessel cooling is permitted & potential sump screen blockage is eliminated.
Low power core (160 MWt)	Reduces decay heat removal requirements	In-vessel retention is enhanced; fission product source term is reduced.
Reactor pool with immersed NSSS and CNV	NSSS and CNV immersed in reactor pool	Enhanced fission product retention and passive long term cooling are provided.
Passive safety systems	Even during the of loss of external power, safety systems cool and depressurize the CNV.	Active safety systems are not required

1.2.3. Holtec International. SMR 160. SMR 160 is an innovative small modular reactor that is designed to run on low enriched Uranium and produces 160 MW electric output. Figure 1.3 shows the schematic of the SMR-160 reactor working. This reactor has an unconditionally safe design as it is designed to contain all its radioactivity irrespective of any conceivable natural or manmade disaster. [9] The design includes a deep underground core and a passive containment cooling system that is responsible for removal of decay heat from the spent fuel pool and from the reactor core in uncommon conditions including station blackouts. SMR 160 also possesses a capability of starting up without having offsite power. [9] The reactor boasts a life span of over 100 years, which is attributed to the absence of boric acid. With a gravity driven thermal hydraulic system, the reactor eliminates a possibility of LOCA's due to pipe ruptures or pump failures.

Along with increasing the safety, this also helps in reducing the operational and maintenance cost for the SMR. As of 2015, Holtec, Inc estimates the cost of installed SMR-160 to be $650 million. This is less than half the cost per megawatt of a large nuclear plant. [9]

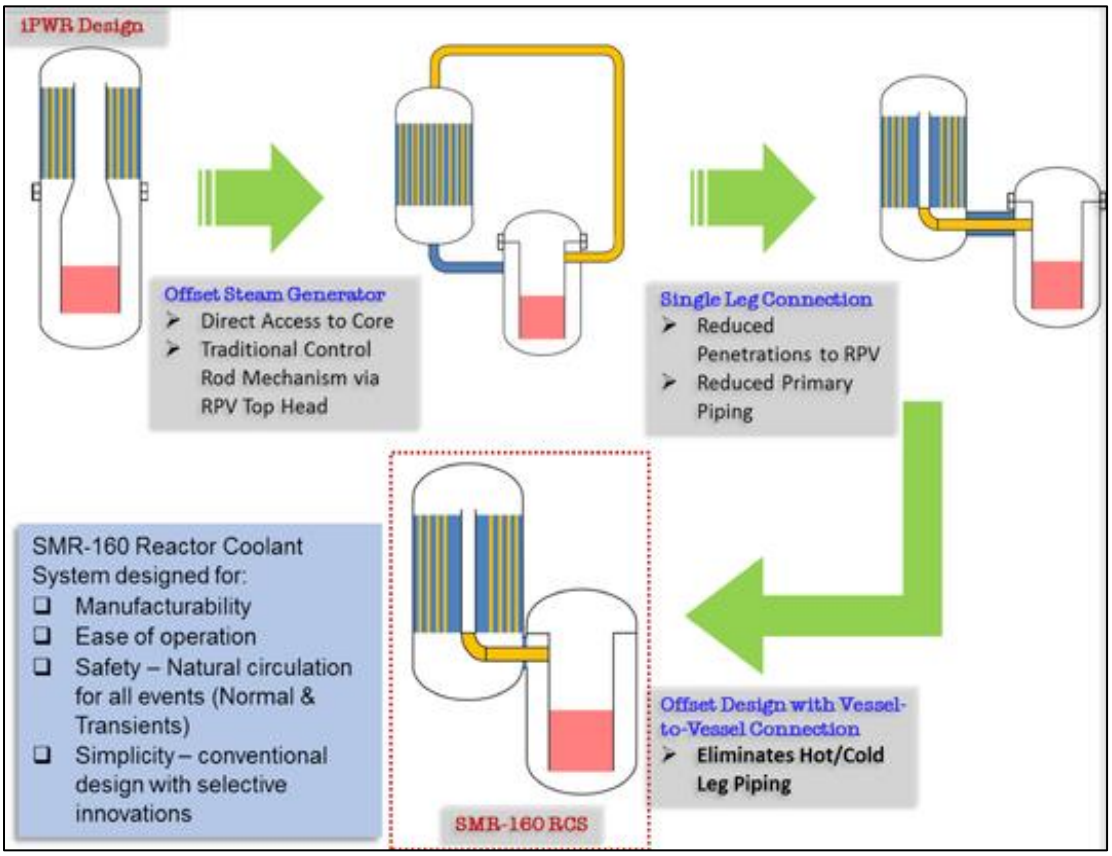

Figure 1.3 SMR-160 working schematic [9]

1.2.4. BWXT Mpower™ Reactor. BWXT technologies, Inc. announced its plan to build this reactor in the year 2009. Figure 1.4 shows the Mpower™ Reactor design model. US department of energy supported the plan for development of this SMR by promising a grant of maximum $226 million in November 2012. As of February 2016, the company has invested more than $375 million towards the development of its Mpower reactor. [5] Like other SMRs, BWXT Mpower™ features an integral design based on a pressurized water reactor. This reactor has a capability of producing an

electrical output of 195 MWe if it is coupled with a water cooled condenser or 168 MWe with an air cooled condenser. [10]

Figure 1.4 BWXT Mpower™ SMR [10]

Table 1.2 shows the various attributes of the Mpower SMR. It can be seen from the design that the reactor has a simplified Nuclear Steam Supply System (NSSS). The integral design eliminates a need of complex and extensive piping system. This reduces or eliminates the possibility of LOCAs. Mpower also features emergency core cooling systems which are based on natural circulation, thus increasing reactor safety.

Table 1.2 BWXT Mpower™ Design Features [10]

Reactor Attributes	Value
Thermal output	575 MWt
Electrical Output	Air-cooled condenser: 168MWe Water-cooled condenser: 195MWe
Vessel Size	Diameter: 13.5 ft. (4.1 m) Height: 90.8ft. (27.5 m)
Vessel Weight (no fuel)	758 tons (688 t_m)
Reactor Coolant Pressure Core inlet temperature Core outlet temperature Core flow	 2150 psi (14.8 MPa) - nominal 555°F (290.6°C) 606°F (318.8 °C) 28.5 Mlbm/hr (3591 kg/s)
Steam Conditions Pressure Superheat Feed Water Temperature	 825 psi (5.7 MPa) 50°F (28°C) @ BOL 414°F (212°C)
Fuel Assemblies	17x17 fuel pin array 94.8" (240.8 cm) active length Less than 5% enriched U^{235} 69 bundles
Reactivity Control	61 CRDMs No soluble boron
Primary Coolant Circulation	8 internal coolant pumps External motors
Emergency Core Cooling Systems	Passive design Natural circulation
Refueling Cycle	24 months On-site spent fuel storage (12 years) without poisoned racks
Steam Generator	Once-through design
Pressurizer	Active (integral electric heaters)

1.3. PASSIVE CONTAINMENT COOLING SYSTEM

In the SMR designs the containment is an integral part of cooling the reactor during accident scenarios through the design of the PCCS. The CNV is partially evacuated during normal operation with a small amount of air present. At the time an accident is initiated, steam is ejected from the Reactor Pressure Vessel (RPV) into the CV. This steam condenses on the containment walls, which are in turn cooled by an external pool of water. This leads to condensation heat transfer from the RPV steam to the containment wall [11]. The condensate is returned to the reactor core through drain lines, where it can continue cooling the reactor core.

1.3.1. W-SMR PCCS. The passive containment cooling system in W-SMR is a compact structure, which can withstand high pressures by design. As shown in Figure 1.5, the containment is submerged in the Outside Containment Pool (OCP). This promotes heat removal from CNV during a loss of coolant accident. The OCP also acts as a radionuclide filter in case of their unlikely escape from the containment. The PCCS is a part of the long-term cooling system, in addition to two Ultimate Heat Sinks (UHS), which can provide additional water inventory to the OCP.

As shown in Figure 1.6, the Automatic Depressurization System (ADS) provides a vent for the reactor steam to flow from reactor side to containment side. This happens in case of an accident when the Core Makeup Tanks (CMT) and In-Containment Pool (ICP) are not able to cool the reactor alone. In such cases, the ADS vents reactor steam, which then condenses on cold containment walls. As condensation takes place on the containment walls, heat is transferred to the OCP and water starts boiling. The OCP, when combined with the water in UHS, can cool the reactor for 7 days. [6] Upon the availability of water from external sources, this can cool the reactor indefinitely.

1.3.2. Nuscale SMR PCCS. The Nuscale SMR PCCS is the Emergencey Core Cooling System (ECCS). As seen by Figure 1.7, it includes three reactor vent valves along with two reactor recirculation valves, which are all independent of each other. The ECCS is said to be actuated when at least two reactor vent valves and one of the two reactor recirculation valves open. [12]

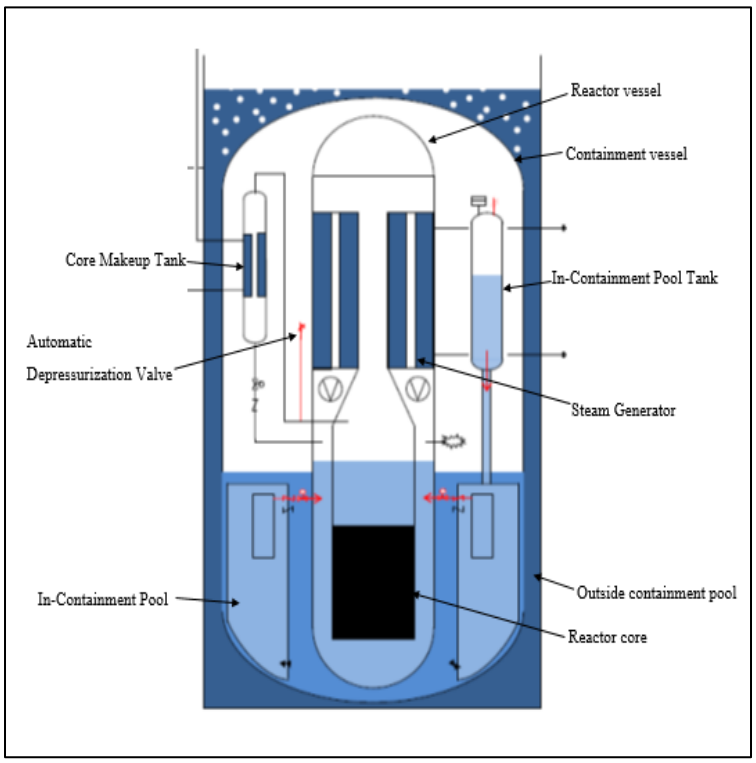

Figure 1.5 W-SMR PCCS [6]

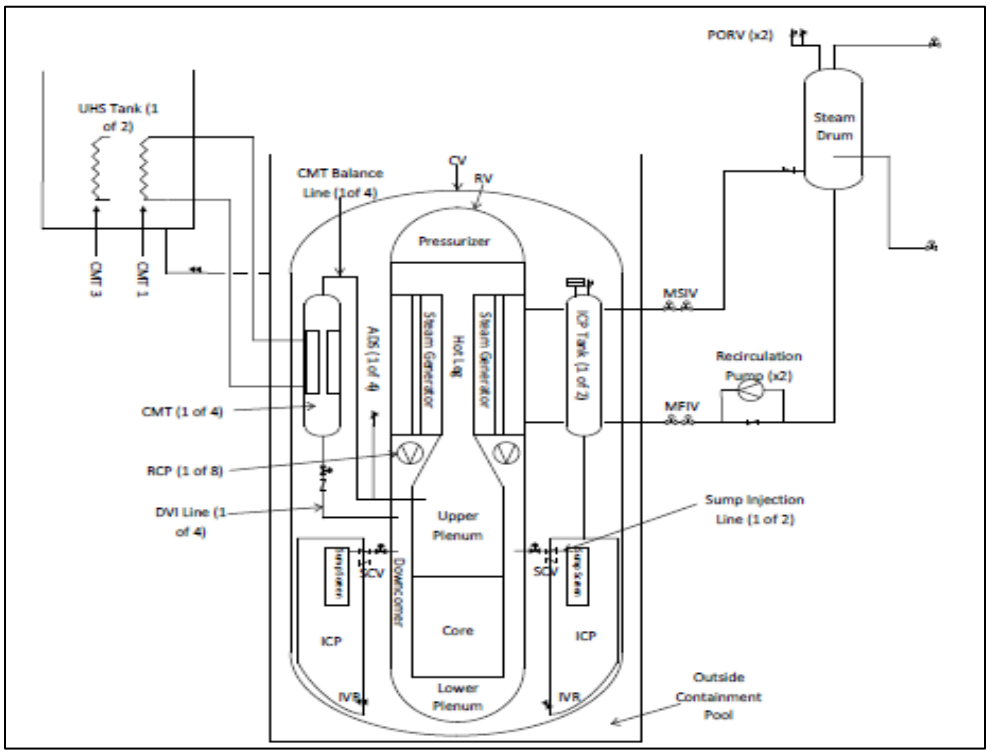

Figure 1.6 W-SMR Reactor coolant and PCCS [6]

In accident scenarios like a loss of coolant accident or other condition resulting in an ECCS actuation, a quick decrease in temperature and pressure takes place due to the removal of heat from the containment vessel. Like the Westinghouse SMR containment, condensation takes place on the inner walls of CNV while it is cooled by conduction and by natural convection of heat. The reactor water pool serves as a heat sink until all the water from reactor pools evaporates. After this point, the natural convection of air is sufficient to cool the reactor. [12]

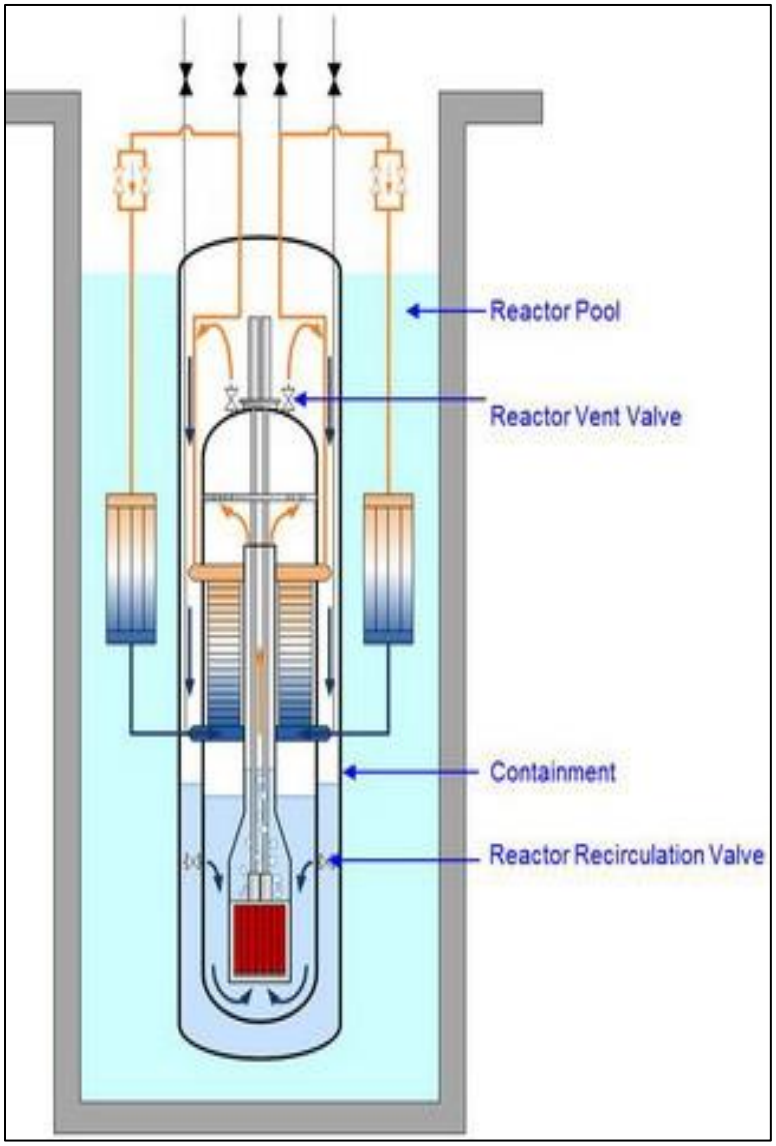

Figure 1.7 NuScale Power ECCS [12]

1.4. PCCS BEHAVIOR ANALYSIS

Kim [13] and Revankar [14] conducted steam-air mixture condensation experiments with secondary side as a pool of boiling water. In the study done by Revankar [14], the experiment was performed on a vertical condenser tube sitting in a pool of water at saturated temperature. This corresponds to a condensation under the constant temperature condition. A strong pressure dependence was found for the heat transfer coefficient (HTC), as it increased almost linearly throughout the pressure range. Vierow [15], Siddique [16] & Kuhn et al [17] performed studies to support the PCCS of GE's Simplified Boiling Water Reactor (SBWR) condenser. This condenser is a heat exchanger composed of vertical steel tubes of 2inch diameter, submerged in a pool of water at atmospheric conditions. Kuhn developed an improved test section to reduce the turbulent perturbations and the developing flow entrance effects. Kuhn's experimental results were in good correlation with the theoretical values but the test was only performed on a 2inch diameter steam tube.

Lee and Kim [18] performed an experimental study on SMR passive residual heat removal system condensers in the presence of nitrogen gas. The heat exchanger tubes used in the experiment had a diameter of 13 mm ID. It was seen that that the influence of Non-Condensable Gases (NCGs) on condensation in a small diameter tube was weak. Also, experiments were only performed at atmospheric pressure. This restricted the scope of empirically developed correlations to unrealistic conditions. It was seen that the Kuhn et al [17] correlation gave a better prediction for larger pipes more than 2 inches in diameter but underestimated the results in this case.

Most previous PCCS relied on heat exchangers with small tube diameters to cool the reactors in case of an accident. However, the proposed W-SMR and other SMR designs rely on cooling the containment vessel, which has dimensions of the order of a few meters. It is therefore required to scale the condensation heat transfer phenomena in vertical tubes in presence of NCGs to predict the characteristics of condensation on containment vessel walls.

1.5. RESEARCH OBJECTIVES

This research aims to study the characteristics of heat transfer of a PCCS in the presence of non-condensable gases. Specific objectives for this research are as follows.

- Review and evaluate existing data and models for condensation heat transfer for application to W-SMR containment condensation
- Perform CFD simulations to evaluate the ability of STAR-CCM+ to predict condensation heat transfer with and without NCGs
- Evaluate the effectiveness of the CFD simulations in scaling of condensation phenomena for different diameter pipes.
- Design a test facility for investigating the scaling of the heat transfer coefficient to larger tube sizes and evaluating the scalability of models for the heat transfer coefficient.

For this purpose, an experimental facility is being created at Missouri S&T. Some key features of the facility include:

- Test section – a condenser system representing the SMR containment.
- 100 kW steam supply to generate steam at pressures up to 667 kPa
- Nitrogen supply – non-condensable gas
- Pressure transducers and thermistors to evaluate thermodynamic state and heat transfer

To date, none of the existing SMR concepts have been licensed or constructed. These objectives, when fulfilled, will provide data necessary to allow scaling of the condensation phenomenon in the containment that can be used in the development and licensing of SMR designs. In the long run, this can provide a safety benchmark for the NRC for SMR PCCS and licensing performance. Figure 1.8 illustrates the scaling of the condensation phenomena to predict the behavior of SMR containment vessel.

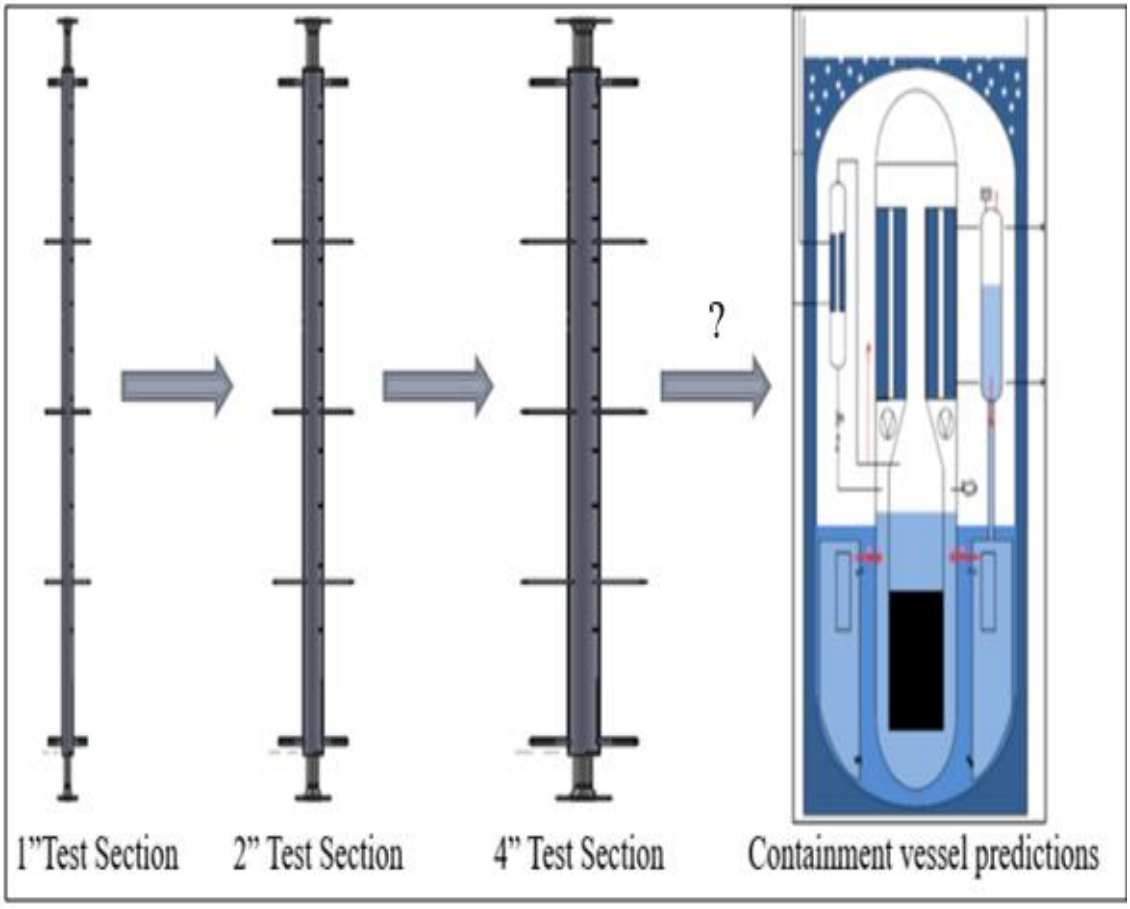

Figure 1.8 Scaling of condensation phenomena

2. STATE OF THE ART

2.1. PREVIOUS STUDIES

It is well documented that even the presence of a slight amount of non-condensable gases (NCGs) greatly influences the condensation process. This fact was first documented by Othmer et al. [11] in 1929. As condensation proceeds in the presence of NCGs, a layer of these gases accumulates at interface of the liquid and vapor. This accumulation of NCGs at the interface forms a diffusion layer which prevents the steam from passing through, it thus causing degradation in the condensation process [17]. This in turn can result in dangerously high pressures inside the CV during an accident if convection heat transfer is insufficient. This might lead to an extremely hazardous situation and thus is also one of the major licensing issues in SMRs. Othmer [11] performed the condensation experiments in a vertical 3 inch tube. The test showed that adding 0.5% air by volume decreased the heat transfer coefficient (HTC) by 50% of the value for pure steam case. A further addition of 0.5% of air reduced the HTC to 1/3rd of the original pure steam value, and so on. [11]

Since the study conducted by Othmer [11], there have been many efforts to better understand the effect of NCGs on condensation for various geometries and thermophysical conditions. A detailed review of these studies can be performed by Huang et al. [19]. It summarized the empirical and theoretical models developed by previous researchers and tabulated the range of thermophysical conditions for different experimental studies.

Before the year 1995, the most prominent efforts were performed by Ogg [20], Vierow et al [15]**,** and Siddique et al [16] while performing experiments to support the research for development of GE's PCCS. [17] All these experiments focused on analyzing the condensation od steam inside vertical tubes, with helium or air as NCGs. The secondary cooling jacket method was adopted for these experiments. The problem for these experiments was that their data was not consistent with each other. This was attributed to the differences in evaluating local CHT and different test section designs. [17]

Kuhn [21] developed an improved test section, as described in the Section 2.1.1, to reduce the measurement inaccuracies and get more reliable results. Since then, there have been a few studies focusing on the effect of a NCG on steam condensation inside vertical tubes. Some of these well cited studies are explained in the Section 2.1.1.

It is important to note that until now, all the experiments were performed for a fixed geometry of the test section. This approach limits the results and the developed correlations to a small range of length scales. Moreover, the analysis of condensation heat transfer in presence of a NCG was done relative to condenser pipe length scales. This restricts the database of CHT characteristics to pipes having an internal diameter of a few inches. However, most SMR containment vessels are of the size of a few meters. It is therefore highly probable that the data from previous literature might not be sufficient to predict the behavior of heat transfer characteristics for condensation heat transfer at the CV walls.

2.1.1. Experimental Studies. Kuhn et. al. [17] focused on studying the characteristics of a Simplified Boiling Water Reactor (SBWR) PCCS condenser. Steam condensation characteristics were evaluated for a 2inch diameter stainless steel vertical tube. The steam was condensed on the inner walls of the tube while the outer walls were cooled by a water jacket. Figure 2.1 shows the schematic of the experimental apparatus used. Steam was provided at a pressure of 135 psia, which was subsequently passed through a separator for the removal of residual moisture and finally supplied to the test section inlet from the top. Water in the annulus was introduced from the bottom and exited from the top. Separator and quench tanks were used at the test section exit to remove any residual steam. Helium or compressed air were used as non-condensable gases. They were heated to a desired temperature and mixed with the steam in proper proportion before entering the test section. [17]

Figure 2.2 represents the detailed sketch of the test-section and the thermocouple placements for Kuhn's experiment. The thermocouples were mounted as shown in detail "A" of Figure 2.2. This was done to reduce the turbulent perturbations that might be caused by the flow across thermocouples. Additionally, nylon spacers were used to keep the tubes concentric. [17] Local cooling water bulk temperature was indirectly measured by measuring the temperature at the outer wall of the 2inch condenser tube along with the

adiabatic wall temperature of water at the same axial location. Local bulk coolant temperatures were then obtained by applying the turbulent convective heat transfer theory.

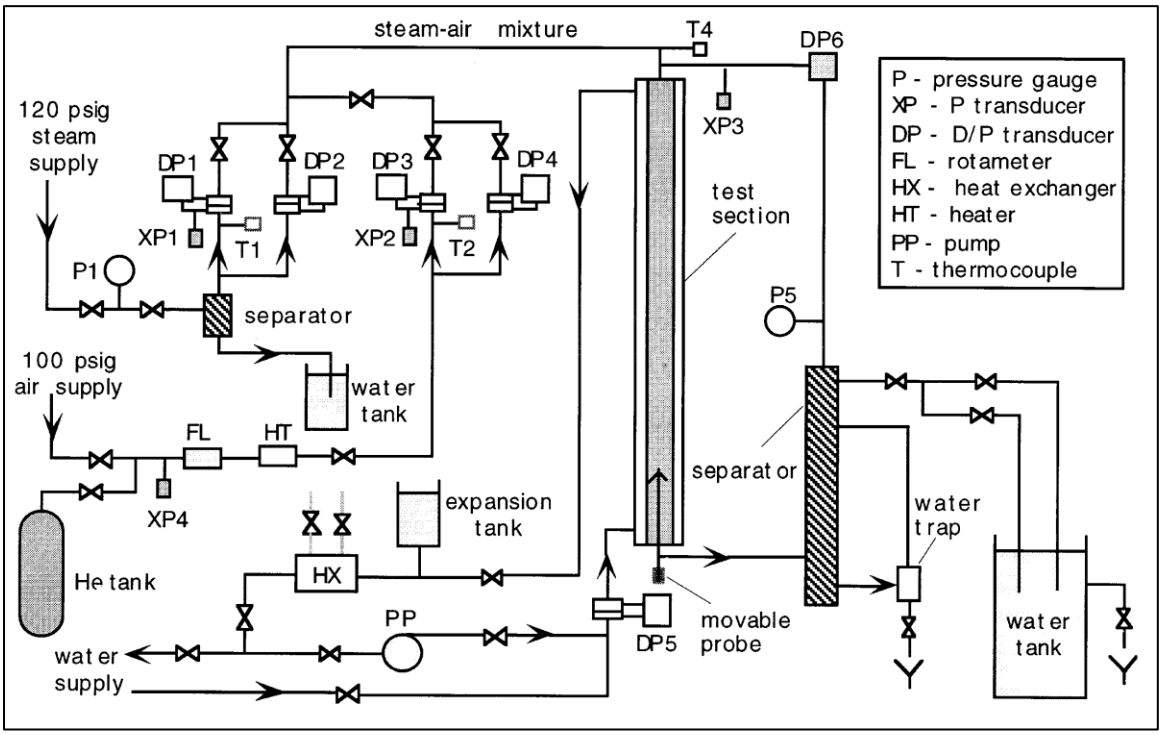

Figure 2.1 Experimental apparatus schematic *[17]*

Vierow [15] and Siddique [16] had performed previous experiments on a PCCS condenser for measuring local Condensation Heat Transfer (CHT) in vertical tubes. The problem for these experiments was that their data was not consistent with each other. This was attributed to the differences in evaluating local CHT and different test section designs. [17]

Three models were generated to predict the results of the experiments, namely the degradation factor method, mass transfer model and diffusion layer theory. In total, the experiments encompassed 71 runs with a steam-air mixture, 42 runs for pure steam and 24 runs for steam-helium mix. The reproducibility of the tests was proved by repeating the tests at 60 days apart.

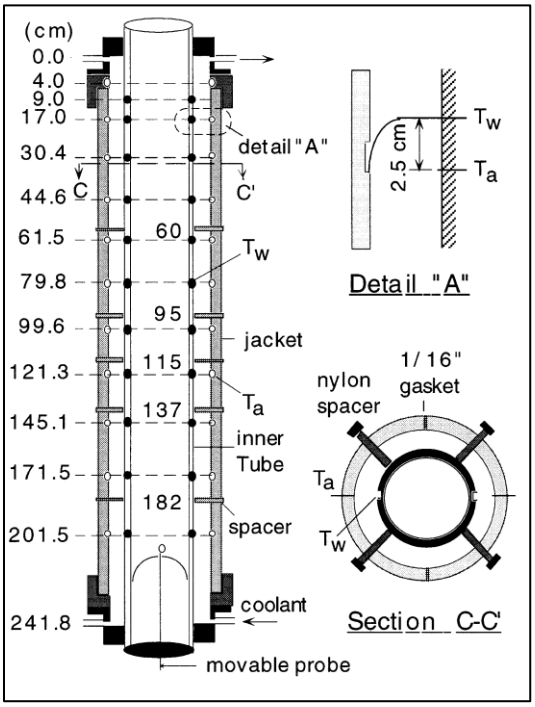

Figure 2.2 Test Section sketch of Kuhn et al. [17]

The degradation factor method was a simplistic approach to calculate a modified degradation factor, which is dependent on Reynolds number. A standard deviation of 7.36% was obtained for the pure steam case, while for the steam-helium mixture and steam-air mixture the standard deviations were 13% and 17.36% respectively. The diffusion layer model considers the condensation and sensible HTCs along with the HTC of the condensate film, thus calculating the suction or blowing parameter to obtain the Nusselt number. The overall HTC obtained from this model showed a deviation of 8.41% and 6.07% for steam-air and steam helium mix, respectively, when compared to the experimental data. [17]

The mass transfer conductance model is also based on the suction parameter calculated from the Couette flow model. An empirical relation was developed based on this model and the experimental data. The initial guess to calculate sensible HTC was provided by the Couette flow model. The total HTC obtained by this model had a standard deviation of 3.24% and 6.38% from experimental data for steam-helium and steam-air cases respectively. Finally, all the models agreed with the experimental results.

Previous literature on GE's SBWR condenser design adopted the secondary water jacket approach. However, Ravenkar [14] argued that the SBWR condensers face a constant temperature boundary condition during a postulated accident, as the surrounding water reaches saturated state. The study provided a novel database for condensation occurring in a vertical tube submerged in water. The water pool on the secondary side acted as a heat sink, to which energy was transferred by the means of boiling heat transfer.

The condenser tube was scaled to half-length and half-diameter for calculating the heat transfer coefficient (HTC). Active length of condensation used for the experiment was .984 m. The experiments were conducted for a steam flow rate of 2.5-5.5 g/s, system pressure of 0.12-0.4 MPa and NCG mass fraction of 0-10%. [14]

It was observed that the HTC decreased with increase in system pressure and with NCG mass fraction, and it increased with increase in mass flow rate of mixture. The error in HTC tended to increase for lower pressure measurements. While theoretically the error could be infinite as the pressure inside the condenser tubes tended towards the secondary side pressure the mean experimental error for all data was found to be 11%. [14]

An analytical model was developed to predict the data for film-wise condensation in the presence of NCG. For developing the correlations, the assumptions of fully developed, ripple free flow were noted. The analogy was based on momentum heat and mass transfer correlations and considers the surface suction effect to develop the correlations. For low NCG mass fraction, the model was found to slightly underestimate the HTC but generally found to predict the data very well. The results from derived correlations were compared to those of the boundary layer model developed by Revankar [22] and were found to give a relative error of 18.7%. In general, it was seen that both analytical and boundary layer models predicted the data very well. The correlations were also seen to agree with the experimental data from Kuhn et al. [17]

Lee and Kim [18] focused on studying the condenser characteristics of Passive Residual Heat Removal System (PRHRS) for the System-integrated Modular Advanced Reactor (SMART). The condenser tubes of PRHRS have a small tube diameter of 13 mm. The test section is therefore constructed to have a condensing tube diameter of 13

mm. Unlike Kuhn et al. [17] and other previous experiments, this experiment uses nitrogen gas as a non-condensable gas. All the experimental data was obtained at atmospheric pressure. This was different from the realistic conditions, as the PRHRS operates at a working pressure of 3.5 Mpa. Theoretical modeling was proposed to obtain the results at actual working pressures. Figure 2.3 shows the schematic diagram of the experimental setup. A gasoline boiler was used to supply the steam at a gauge pressure between 0.3 and 0.5 Mpa. A surge tank was used to reduce the effect of fluctuations in pressure on the mass flow rate of steam. [18] A moisture separator was used to obtain saturated steam at the given pressure. Nitrogen was preheated and mixed to the steam in desired quantity before entering the test section.

Figure 2.4 shows the sectional view of the test section. The condenser tube is a 3 m long stainless steel tube of 13 mm inner diameter and 2.5 mm thickness. 13 K-type thermocouples were soldered to the outer surface of the condenser tube at different axial locations.

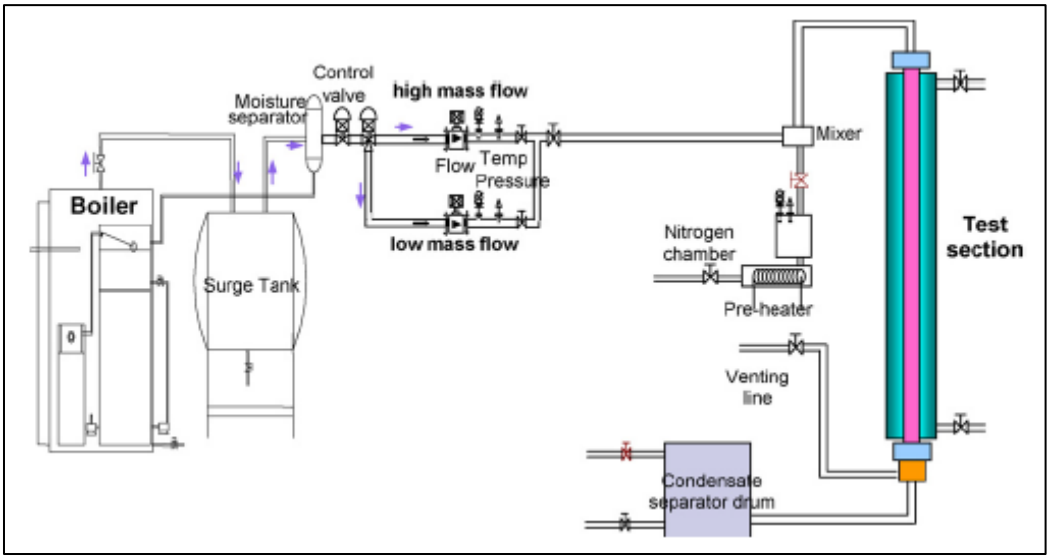

Figure 2.3 Experimental setup schematic [18]

The outer water jacket is made of 3 blocks of acrylic measuring 1meter long each, stacked on top of each other. The bulk temperatures of cooling water were measured at 11 axial locations in the acrylic jacket. Like Siddique [16], this experiment used air bubbles in the cooling water to induce turbulence. The transparency of the acrylic tube

helped to maintain the desired slug flow regime in the annulus, which is required for proper mixing.

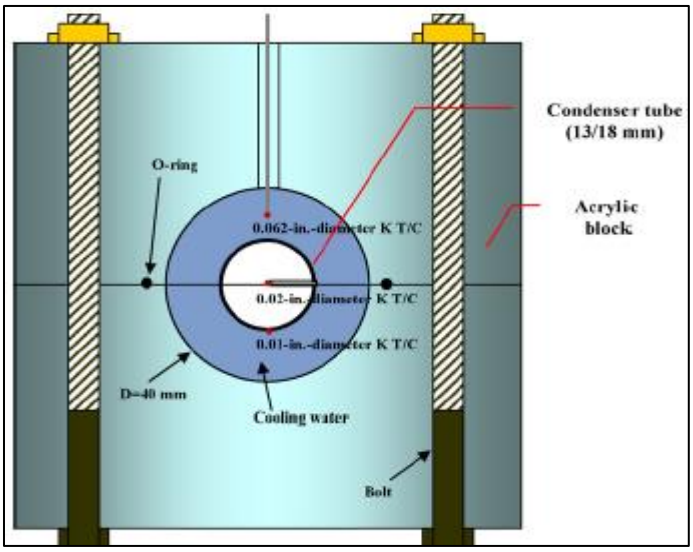

Figure 2.4 Sectional view of the test section [18]

Pure steam experiments were performed at an inlet flow rate of 6.5 to 28.2 kg/hr steam mass flow rate. In such cases, the major resistance to heat transfer is offered by the fluid film. Steam/ Nitrogen tests were performed for nitrogen mass fractions ranging from 3 to 40 percent. Figure 2.5 shows the variation of the condensation heat transfer coefficients for a flow rate of 11.2 kg/hr. [18] It was seen that the local heat transfer coefficient was reduced as the mass fraction of nitrogen increases. Another key observation made by Lee and Kim [18] was that steam-nitrogen mixtures with smaller nitrogen mass fraction behaved the same as pure steam cases. This was only observed in small diameter tubes used in this experiment. Larger diameter tubes showed a significant impact of even small concentrations of non-condensable gases, as shown by previous literature. [18] Lee and Kim also proposed a correlation for prediction of heat transfer coefficient as summarized in Table 2.1 of Section 2.2. Although this was a simplistic relation as compared to Kuhn's [21] correlation, it captured the effect of pipe diameter on the overall HTC within a certain range.

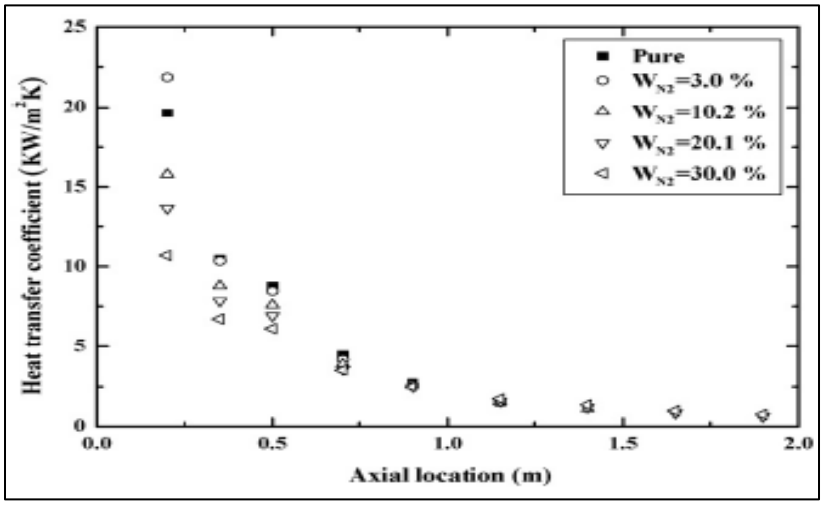

Figure 2.5 Heat transfer coefficient for different nitrogen mass fractions [18]

2.1.2. Computational Studies. Jun-De Li [23] performed a CFD analysis of condensation in the presence of non-condensable gases in a vertical cylindrical tube. ANSYS FLUENT software was used to model the test section and simulate results in various input conditions. The liquid condensate film was modelled by using the Nusselt approximation to save computational resources and time. [23] As the FLUENT version used for the study only allowed for a single mixture material for simulating the whole domain, the heat transfer simulations between two separate multispecies fluid regions could not be performed synchronously. [23] Therefore, separate simulations were performed for the condenser and the cooling water channel regions. The two simulations were solved iteratively with the output file of one acting as an input file for other, until convergence was achieved. The coupling of two simulations was achieved at the inside cylindrical surface of the stainless steel condenser tube. This asynchronous iterative simulation process was started by guessing the wall temperatures at cell centers for the condenser side. [23]

Simulations were performed for studying the condensation of steam with air acting as a non-condensable gas. The mass fraction of steam at inlet ranged from 66 to 98 percent. The ideal gas assumption was used for the gas mixture and its thermal properties were allowed to vary with changes in temperature. The effect of buoyancy forces arising

owing to fluctuations in mass fraction and temperature was not neglected for simulating gas mixture, while the Boussenisq approximation was used for the cooling water side.

Results from the FLUENT simulations were validated against the experimental results of Kuhn [21]. It was seen that the bulk(centerline) temperature of the steam-vapor mixture and the adiabatic wall temperature from CFD results were in general agreement with that of Kuhn data [21]. It was found that heat transfer in cooling channel was the limiting factor for high steam mass fraction cases. The CFD results showed a complex profile for the variation of heat flux while the heat flux from Kuhn's data [21] was able to fit a third order polynomial. The simulation results showed that average axial velocity decreased quickly as the steam condensed. It was also seen that the gas mixture density increased both axially and radially along the condenser tube.

Zschaeck et al. [24] performed a CFD study to validate their proposed mathematical model which was used to predict wall condensation in the presence of NCGs. The simulations were performed in Ansys CFX 14.0 and were validated against the results from 2 different experimental studies. The model used mass sinks, applied to the multi-component gas, on wall boundaries and at conjugate heat transfer interfaces to simulate condensation. This study did not model the details of the liquid film, and phenomena of re-evaporation and condensation accumulation are neglected. At the conjugate heat transfer interface, it was assumed that the latent heat of condensation is absorbed by the solid material. [24]

The CFD analysis was performed on two types of duct cross-sectional geometries. The first study was performed on a square duct and the second on a cylindrical duct. [24]. The cylindrical case was compared with the results from Kuhn et al. [17]

ANSYS DesignModeler 14.0 was used to construct the geometry for simulations. While Kuhn's [17] geometry has two axisymmetric inlets and 4 outlets, Zschaeck et al. [24] made the geometry assuming 90^{o} symmetry. Figure 2.6 represents the geometry used for CFD analysis. A two dimensional study was performed to identify the special discretization error followed by a three dimensional study.

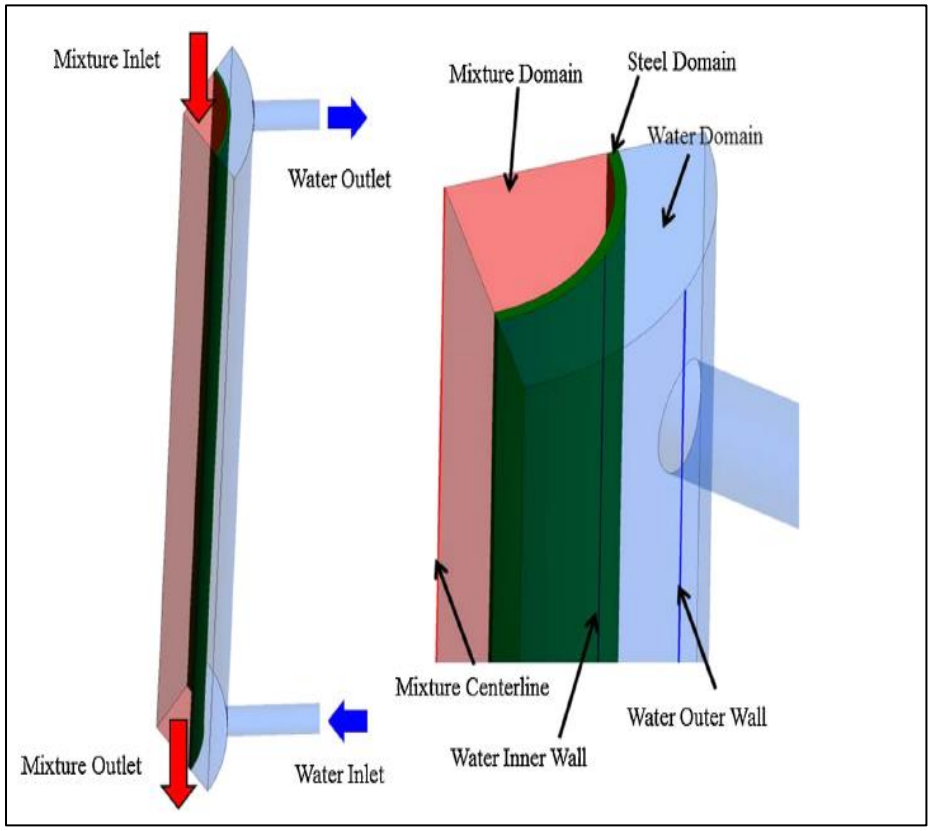

Figure 2.6 Three-dimensional model of geometry used for simulations [24]

Mesh convergence was achieved and it was shown that for both two dimensional and three dimensional simulations, the drop in centerline temperature of condenser tube was more pronounces in experiments as compared the CFD results. [24] This was attributed to the fact that turbulent intensity and the turbulent viscosity ratio were not provided by Kuhn et al. [17]

Figure 2.7 compares the results from two dimensional and three dimensional CFD simulations for the best mesh size to the experimental data from Kuhn et al. [17]. It was seen that three dimensional analysis gave a better representation of temperature profile for the inner wall of cooling jacket. [24] The initial drop in water inner wall temperature was expected as it had to match the inlet water temperature, while the deviation in CFD and experimental results for Z >1.8 meter was not accounted for. It was hypothesized that the deviation might be due to unaccounted heat losses in the experiment. [24]

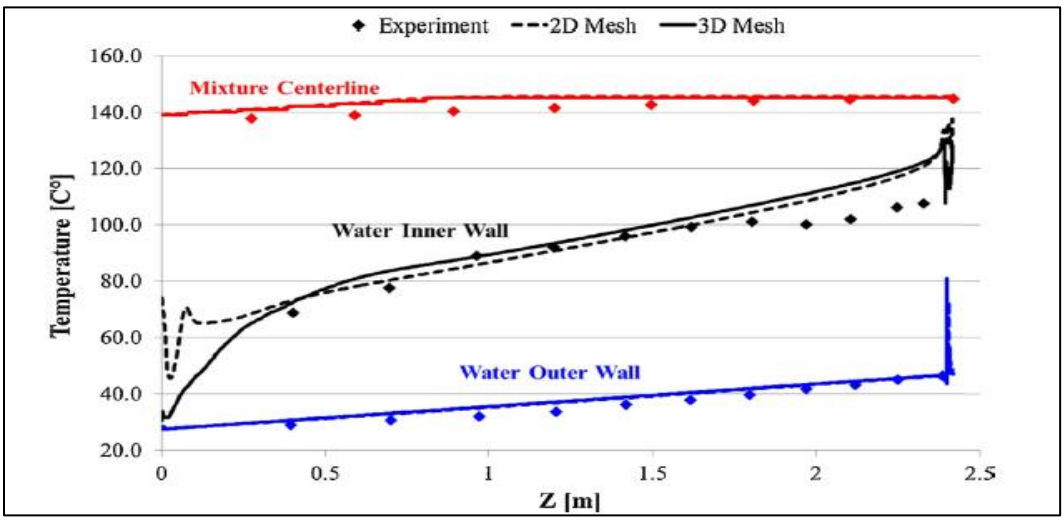

Figure 2.7 Temperature profiles for best mesh size of 2D and 3D simulations [24]

Fu et al. [25] performed simulations using ANSYS/Fluent to model steam condensation in vertical tubes, using helium and air as non-condensable gases. Source terms were defined for each of the conservation equations, including mass, momentum and energy, to model the condensation phenomena. A source term was also defined for individual species conservation equations. The geometry was based on the Kuhn et al. [17] experiment. A two-dimensional axisymmetric model was used instead of a three dimensional geometry and the simulations were performed only in steady state. Fu et al. [25] did not model the liquid condensate film in the fluid domain and instead used the source terms in the wall adjacent cells to simulate the condensation. The mesh was refined to make the near wall y^+ to be less than 1. [25]

For the boundary conditions, a mass flow inlet was used with a uniform temperature and mass fraction. Outlet of the steam/vapor mix was specified as a pressure outlet. Kuhn's [21] data was used to extrapolate the temperatures of gas-liquid interface as a polynomial function. The liquid-gas interface temperatures were calculated from the inner wall temperatures depending upon the film thickness, heat flux and film thermal conductivity. Figure 2.8 shows the extrapolated liquid-gas temperatures calculated according to Kuhn's experimental run number 2.1-13R.

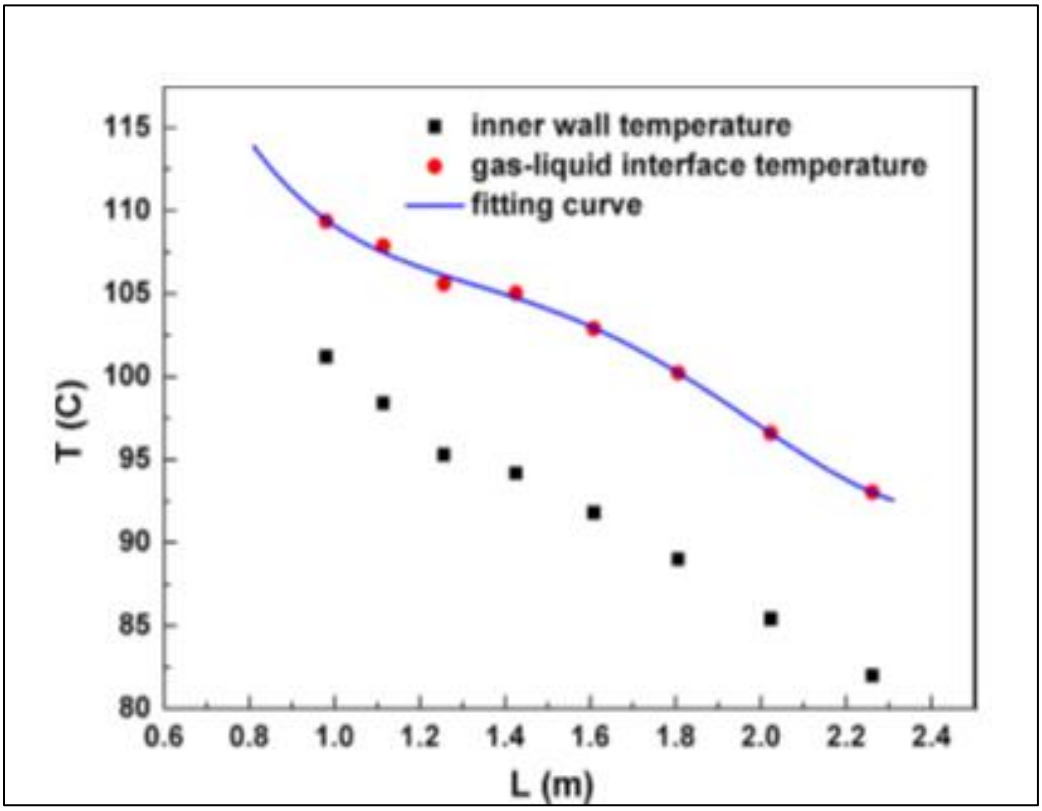

Figure 2.8 Extrapolated liquid-gas interface temperature [25]

The results were compared with Kuhn's [21] experimental data by looking at the steam/vapor centerline temperature and heat flux at various axial locations. It was seen that the simulations were in general agreement with the experimental data. Fu et al. [25] reported an increase in both convection and condensation Heat Transfer Coefficients (HTCs) with increase in steam mass fraction. It was seen that for steam mass fractions of less than 5%, the convection HTC was comparable to condensation HTC, while for larger steam mass fractions, condensation HTC was dominant. [25] Figures 2.9 and 2.10 show the comparison of Simulation results for steam-air and steam helium cases respectively with Kuhn's [21] experimental data. It was seen that both centerline temperature and heat flux follow the same trend as shown by the experiments.

A radial velocity was seen in the simulations, causing the suction effect of condensation. Fu et al. [25] reported an increase in suction effect on mass and heat transfer for increasing steam mass fractions. It was also observed that changing the Reynolds number did not affect the suction effect. Condensation was simulated with

either air or helium as non-condensable gases. The mass transfer for steam-helium mixture was found to be generally greater than the steam-air case. This was attributed to fact that helium offers less resistance to the diffusion of steam as compared to air. However for high inlet steam mass fraction (greater than 90%) it was found that condensation mass flux for both helium and air simulations was almost same.

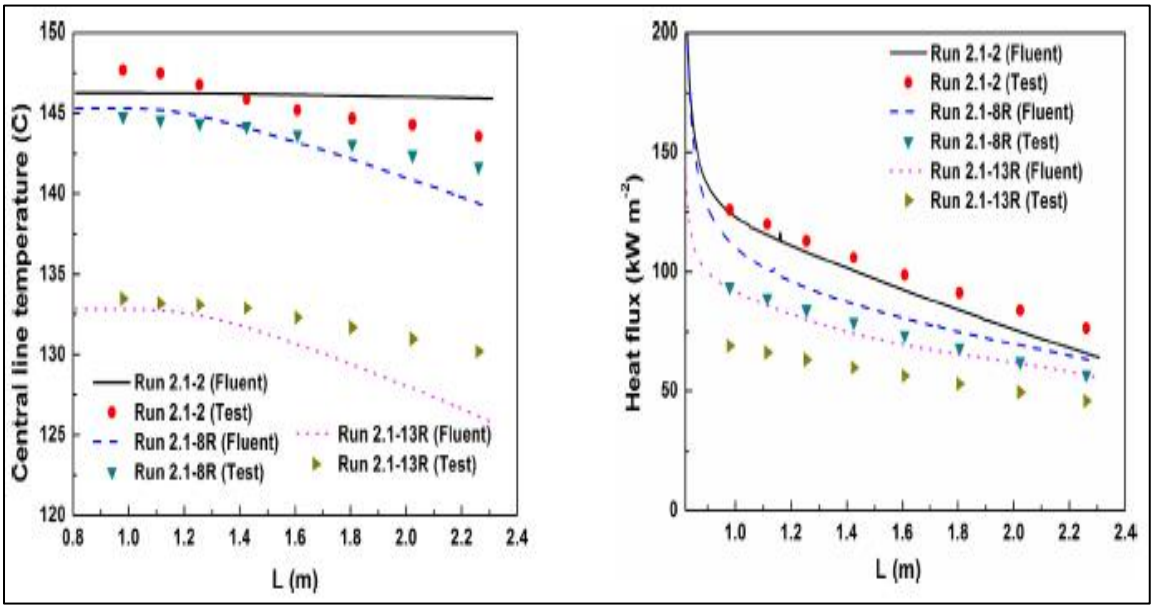

Figure 2.9 Simulation vs experimental results for steam-air mixture [25]

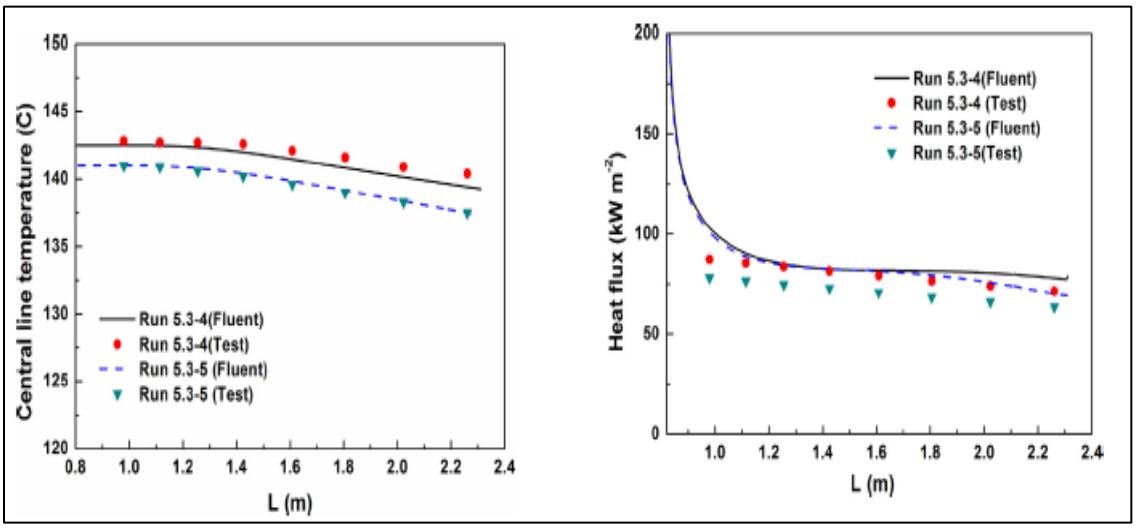

Figure 2.10 Simulation vs experimental results for steam-helium mixture [25]

2.2. MODELS AND CORRELATIONS

Table 2.1 shows various empirical correlations derived by the authors for their studies and it is evident by looking at the constants and validity ranges that these correlations are specific to the conditions under which that experiment was performed and cannot be generalized to be predict the heat transfer characteristics in other conditions.

Table 2.1 Proposed Empirical Correlations *[18]*

Authors	Empirical Correlations	Correlation Parameters & Validity Range
Vierow and Schrock [26]	$f = \frac{h_{exp}}{h_{Nu}} = f_1 . f_2 = \left(1 + aRe_{mix}^{b}\right).(1 - cW_{nc}^{d})$,	$a=2.8x10^{-5}$, b=1.18, c=10 for $W_{nc}<0.063$; and d=0.13 for $0.063<W_{nc}<0.6$; c=1.0 and d=0.22 for $0.6<W_{nc}$
Siddique et al. [16]	$Nu = CRe_{mix}^{a} . \left(\frac{W_{nc,w} - W_{nc,b}}{W_{nc,w}}\right)^{b} Ja^{c} Sc^{d}$,	Where C=6.123, a=0.223, b=1.144, c=-1.253 and d=0.0
Kuhn [21]	$f = \frac{h_{exp}}{h_{Nu}} = f_1 . f_2 = f_{1,shear} . f_{1,other} . f_2 = \frac{\delta_{shear}}{\delta_{Nu}} . \left(1 + aRe_f\right).(1 - bW_{nc}^{c})$	Where $a=7.321x10^{-4}$, b=2.601, c=0.708 for $W_{nc}<0.1$; b=1.0 and c=0.292 for $0.1<W_{nc}$
Lee and Kim [18]	$f_{mix} = \frac{h_{exp,mix}}{h_{Nu}} = \tau_{mix}^{*0.3124} (1 - 0.964 W_{nc}^{0.402})$	For $0.06 <\tau^{*}mix<46.65$ and $0.038<Wnc<0.814$

2.2.1. STAR-CCM+ Documentation. STAR-CCM+ models condensation in a fluid film as a gas or its component condenses on a surface. Film-physics continuum interaction models together with the evaporation and condensation model have to be activated for simulating condensation in the fluid film. [27] As a gas component condenses on a cool surface, the film thickness increases. This model can also be used to model film evaporation from a heated surface.

The fluid film needs a shell region to be specified and allocated to the film physics before it can be simulated. This shell region is a space between the condensing gas and the surface on which it needs to condense. This shell region is created from the boundary of an existing region. It is essentially a two-dimensional region as it is only one cell thick and its boundaries are specified as edges. [27] For condensation on a solid wall, connectivity of the shell region to the solid surface has to be maintained by creating an interface between them. In contrast, an interface is automatically created on the surface of the shell region interacting with the gas phase.

The fluid film is modeled in STAR-CCM+ such that the mass flux of every species is conserved at the interface between a multi-component gas and the fluid film region. Equation 1 represents this conservation of mass formulation. [28]

$$\rho_{g_s} Y_{g_{s,i}} \left(v_{g_s} - \dot{h}\right) - \rho_{g_s} D_{g_{s,i}} \frac{dY_i}{dy}|_{g_s} = \rho_{l_s} Y_{l_{s,i}} \left(v_{l_s} - \dot{h}\right) - \rho_{l_s} D_{l_{s,i}} \frac{dY_i}{dy}|_{l_s} \qquad (1)$$

Subscript "s" refers to the surface where equation 1 is evaluated. ρ_{g_s} and ρ_{l_s} represent the gas and liquid phase densities respectively. Similarly, the mass fractions for the gas and liquid film are represented by $Y_{g_{s,i}}$ and $Y_{l_{s,i}}$. The rate of change of film thickness is $\dot{h}$ and the normal velocity components of gas and liquid film are v_{g_s} and v_{l_s} respectively. Molecular diffusion coefficients for gas and liquid film are written as $D_{g_{s,i}}$and $D_{l_{s,i}}$. [28]

Along with the interfacial mass conservation, the total mass is also conserved and is given by the equation 2. Equation 3 gives the formulation of evaporation rate. [28] The negative value of this quantity can be considered as the condensation rate.

$$\rho_{g_s} \left(v_{g_s} - \dot{h}\right) = \rho_{l_s} \left(v_{l_s} - \dot{h}\right) \qquad (2)$$

$$\dot{m}_v = -\rho_{l_s} \dot{h} \qquad (3)$$

Component evaporation rate is expressed by Equation 4, and Equation 5 gives the expression for interfacial heat flux.

$$\dot{m}_{v,i} = Y_{g_{s,i}} \dot{m}_v - \rho_{g_s} D_{g_{s,i}} \frac{dY_i}{dy}|_{g_s} \qquad (4)$$

$$k_g \frac{dT}{dy}|_{g_s} - k_l \frac{dT}{dy}|_{l_s} - \dot{Q}_v = 0 \qquad (5)$$

In the above equation, k denotes thermal conductivity and $\dot{Q}_v$is given by Equation 6, where $N_v$is the number of interacting components.

$$\dot{Q}_v = \Sigma_i^{N_v} \Delta H_i^{vap} \dot{m}_{v,i} \tag{6}$$

STAR_CCM+ models condensation either by a hydrodynamically limited or a thermally limited approach. The hydrodynamically limited model deals with condensation occurring below saturation temperatures, while the thermally limited case is for condensation at the saturation temperature of the gas.

For condensation taking place below the saturation temperature, STAR-CCM+ iteratively solves for interfacial temperature (T_s) through the secant method, such that Equation (7) is satisfied. [29]

$$f(T_s) = k_g \frac{dT}{dy}|_{g_s} - k_l \frac{dT}{dy}|_{l_s} - \dot{Q}_v(T_s) \tag{7}$$

Equation (8) details the iterative solution used for calculation of T_s, for values of n ranging from 3 to N_{it}. [29] Before solving the equation (8), $f(T_0)$ and $f(T_1)$ are calculated from $T_{s,0}$and $T_{s,1}$. [29]

$$T_{s,n} = T_{s,n-1} - f_{n-1}\left(\frac{T_{s,n-1} - T_{s,n-2}}{f_{n-1} - f_{n-2}}\right) \tag{8}$$

STAR-CCM+ uses the value of $T_{s,0}$ as the actual interfacial temperature at the optimizer entrance and $T_{s,1}$is taken to be five percent below $T_{s,0}$.

For condensation at saturation temperature, T_{sat} limits the calculation of T_s as mentioned above. The saturation state can be identified by checking if Equation (9) or Equation (10) or both of them are satisfied.

$$\Sigma_i^{N_v} Y_{g_{s,j}} = 1 \tag{9}$$

$$\Sigma_i^{N_v} Y_{g_{\infty,j}} = 1 \tag{10}$$

Equation (9) is the mathematical representation of the statement that the interface temperature is equal to the boiling temperature. The interfacial mass fraction of gas is denoted by $Y_{g_{s,j}}$. Equation (10) states that for a pure vapor, only a quasi-steady equilibrium can be reached at the interface as its temperature reaches the saturation temperature. [29]

For CFD simulations involving steam condensation on dry walls, the film heat transfer coefficient is approximated by Equation (11), where k_f represents the film thermal conductivity and h denotes the film thickness.

$$k_l \frac{dT}{dy}|_{l_s} \sim \frac{2k_f}{h}(T_{l,c} - T_s) \tag{11}$$

It can be seen that for negligible film thickness, such as the at the beginning of a simulation, Equation (11) predicts infinite heat flux. This causes the simulations to diverge. To rectify this a dropwise condensation model is used which behaves like a hydrodynamically limited model. This model uses a multiplying factor f_A as given by Equation (12) to calculate condensation rates when f_A is smaller than 1.

$$f_A = 2\pi N R_{eff}^2 \tag{12}$$

The model requires 2 additional parameters as shown in Equation (12). N is specified as N_seeds under the evaporation/condensation physics model in the software. This represents the droplet seed density on the walls. R_{min} is the minimum radius of the nucleated droplets which is specified as R_seeds in the software.

2.2.2. Relap5 (3D) Documentation. RELAP5-3D is a widely used software code developed by Idaho National Laboratory to model the thermal hydraulic and kinetic characteristics of water cooled nuclear reactors. It is the extension of the one dimensional RELAP5/MOD3 code. RELAP5-3D is capable of simulating multidimensional reactor thermal hydraulics characteristics in transients and accident scenarios. [30]

Wall condensation is modeled in RELAP5-3D as a laminar film. The current capability of the software is limited to modeling the laminar fluid film condensation in vertical or inclined surfaces and inside horizontal tubes with a stratified flow regime. [31] The condensation model in RELAP5-3D follows a logical process to calculate the wall heat transfer coefficient accurately and to achieve convergence in the code. The built in assumptions require the wall temperature to be lower than the bulk saturation temperature by at least 0.001 K. It is also assumed that condensing film temperatures are higher than wall temperature. The condensation model transitions to a forced convection model for liquid volume fractions lower than 0.1. Furthermore, it is required for the quality of bulk NCGs to be less than 0.999 and the pressures to be below the critical pressure limit. [31]

The condensation heat transfer coefficient calculated by RELAP5-3D leads to prediction of total heat flux as given by Equation (13). The total heat flux is represented by q_t",while h_c is the predicted condensation HTC. Based on the bulk vapor partial pressure, the wall temperature and the saturation temperature are given by T_w and T_{sppb} respectively. [31]

$$q_t" = h_c(T_w - T_{sppb}) \tag{13}$$

The condensation model in RELAP5-3D allows the heat flux from wall to both liquid film and gas/vapor mixture. Equation (14) gives the heat flux to the liquid film, and this can be subtracted from the Equation (13) to obtain the heat flux to vapor/gas mix. Here, T_f is the bulk fluid film temperature. The wall heat flux to the vapor/gas is either zero or a negative quantity. [31]

$$q_f" = h_c(T_w - T_f) \tag{14}$$

For inclined surfaces, the condensation HTC is calculated from the maximum of Nusselt's [32] correlation which is valid for laminar flow regime and Shah's [33] correlation, valid for turbulent regime. From Equation (15), it can be seen that the Nusselt [32] correlation uses film thickness, δ, as a key parameter for calculating heat transfer coefficient instead of temperature difference. The thermal conductivity of fluid film is represented by k_f.

$$h_{nusselt} = \frac{k_f}{\delta} \tag{15}$$

Shah's [33] correlation, used to calculate the condensation heat transfer coefficient, is represented by Equation (16). Here Z is given by Equation (17) and h_{sf} is the superficial heat transfer coefficient.

$$h_{shah} = h_{sf}(1 + \frac{3.8}{Z^{0.95}}) \tag{16}$$

$$Z = (\frac{1}{X} - 1)^{0.8} P_{red}^{0.4} \tag{17}$$

X is the ratio of the sum of vapor and NCG mass to the total mass (including vapor, NCG and liquid film mass). P_{red} is the reduced bulk pressure and is defined as the ratio of bulk pressure to the critical pressure. $h_{sf}$is related to the Dittus-Boelter coefficient h_1 by Equation (18).

$$h_{sf} = h_1(1 - X)^{0.8} \quad (18)$$

The Dittus-Boelter coefficient in above equation assumes that all fluid is liquid. h_1 can be defined in terms of hydraulic diameter D_h, thermal conductivity k_1, Reynolds $Re_1$and Prandtl number Pr_1 by Equation (19)

$$h_1 = 0.023(\frac{k_1}{D_h})Re_1^{0.8}Pr_1^{0.4} \quad (19)$$

Shah correlation comprises of the data from both vertical and horizontal cases. RELAP5-3D computes the maximum of $h_{shah}$and $h_{nusselt}$ as the wall condensation heat transfer coefficient h_c. Table 2.2 gives a brief comparison of the fluid film condensation modeling approach used by STARCCM+ and RELAP5-3D.

Table 2.2 Condensation modeling comparison between STARCCM+ and Relap5-3D

STARCCM+	**RELAP5-3D**
Three dimensional CFD code	One dimensional code
Based on mass, momentum and energy conservation (theoretical models)	Based on Shah's and Nusselts correlation. (empirical, more practical)
Hydrodynamically limited or thermally limited based on mass and interfacial heat flux balance.	Calculates maximum condensation heat transfer coefficient to find heat flux.
Modeled as laminar film	Modeled as laminar film
Coupled wall and interfacial heat transfer –code automatically calculated energy to the fluid film and to wall from bulk steam/air	Uncoupled wall and interfacial heat transfer rates –energy from steam-gas region equals the energy transferred to wall (condition enforced)

3. EXPERIMENTAL APPARATUS

The schematic drawing of experimental facility is shown in Figure 3.1. The setup consists of a test-section instrumented with thermistors and pressure transducers, steam and nitrogen supplies metered by a vortex flow meter and laminar flow meter, respectively, and a preheater for nitrogen and a pre-cooler for the throttled steam-nitrogen mixture. Pressure and temperature gauges will be used to measure thermodynamic properties of the inlet mixture as shown in Figure 3.1 The building steam system is used to obtain saturated steam at 100 psia. An open loop configuration was used for the steam side and a closed loop was used for the cooling water circulation. The steam pressure and flow rate is controlled using a chain wheel type globe valve.

The geothermal cooling system of the building was used to obtain the required cooling water at a set temperature. Besides being used in the secondary water jacket of test section, cooling water was used to pre-cool the throttled steam-nitrogen mixture to saturation temperatures. Also, a part of the cooling water was used in the exit side heat exchanger to completely condense the steam and to sub-cool it below 120^{o}F before sending the condensate to the drain.

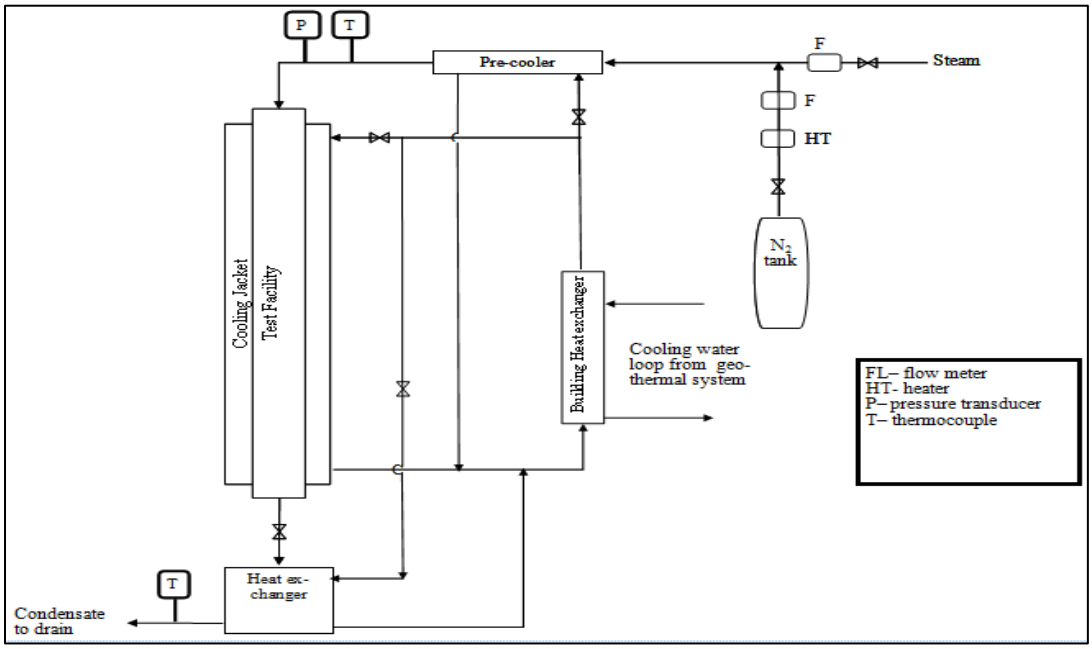

Figure 3.1 Schematic of experimental apparatus

Figure 3.2 shows the sectional front view of the test section. The test section was a tube in tube heat exchanger installed in a counter flow configuration. Steam enters the condensing tube at the top and condensate leaves from the bottom. Water flows into the ccoling jacket from two inlets at the bottom and exits from 2 outlets at the top. Both inlets and outlets are circumferentially opposite to each other. For the 1 inch test section, the condenser tube is made out of a 1 inch Schedule 10 pipe having a total length of 106 inches. The water jacket is made from a 96 inch long, 2 inch Schedule 40 pipe.

As shown by Figure 3.3, a total of 48 thermistors will be installed, at 12 axial and circumferencially opposite locations to measure the temperature of inner wall of water jacket and outer wall of the condenser tube. The coolant bulk temperature will then be calculated from these two temperatures using the theory of turbulent convective heat transfer. The thermistor placement positions were calculated to prevent a potential source of error from measurement tolerance of closely spaced thermistors as shown in Figure 3.4. The detail "C" in Figure 3.4 shows an indentation mark created on the condenser tube outer wall to ensure proper contact with the thermistor and help reduce potential measurement error.

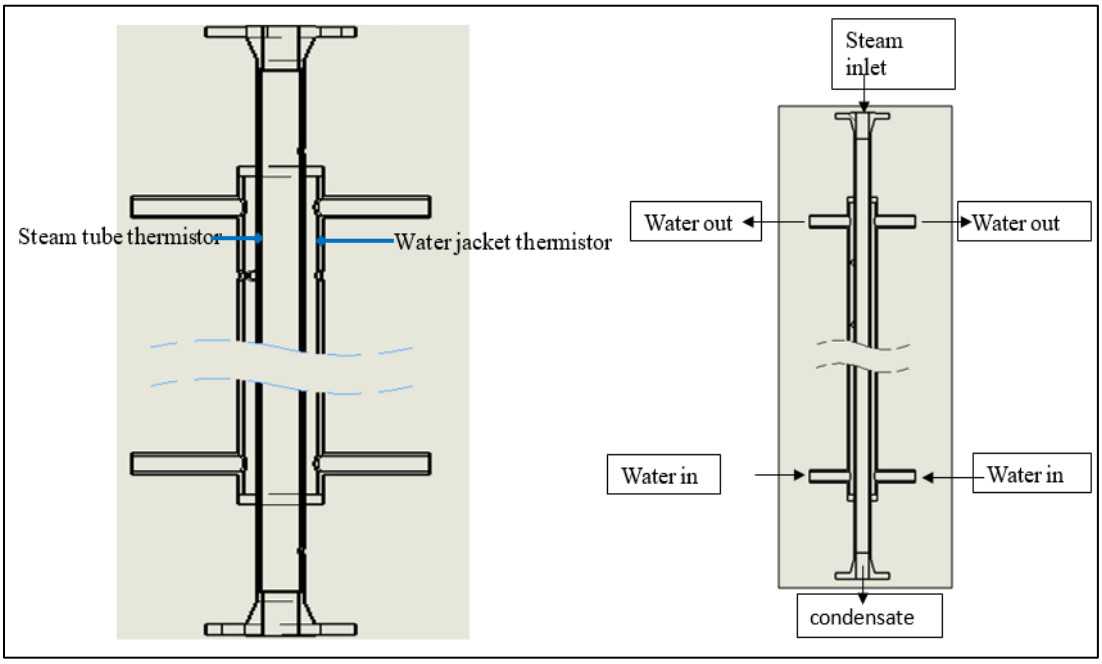

Figure 3.2 Test section schematic

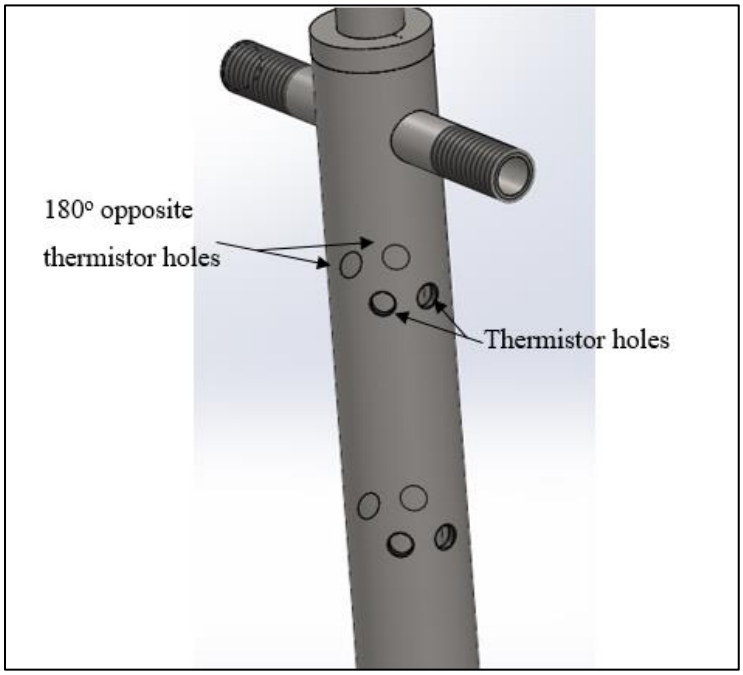

Figure 3.3 Drilled holes for thermistor placement

The placement of thermistors was calculated so as to minimize uncertainty in the thermistor measurements. Based on the thermistor tolerance of ±0.2°C, Equations (20) and (21) were used to calculate the minimum axial distance for the thermistor placement so that the error in the measurements is small compared to the temperature difference. Azimuthal symmetry of temperature was assumed.

$$dq = mc_p dT(z) \tag{20}$$

$$dq = UAdT(r) \tag{21}$$

Solving the above two equations, we get Equation (22), which relates the temperature to the axial distance.

$$T_z = T_{in} - (T_{sat} - T_{in}) * \exp(-\alpha * z) \tag{22}$$

$$\alpha = constant \tag{23}$$

α is based on the fluid properties and geometry of the system, c_p represents the specific heat of water and U denotes the overall heat transfer coefficient given by the resistance circuit analogy. Convective resistance of steam and conductive resistance the 304 stainless steel wall of steam pipe, are combined to form the overall heat transfer coefficient. In all, 44 thermistors will be used to measure the water temperature and the outside temperature of the steam tube at different axial locations.

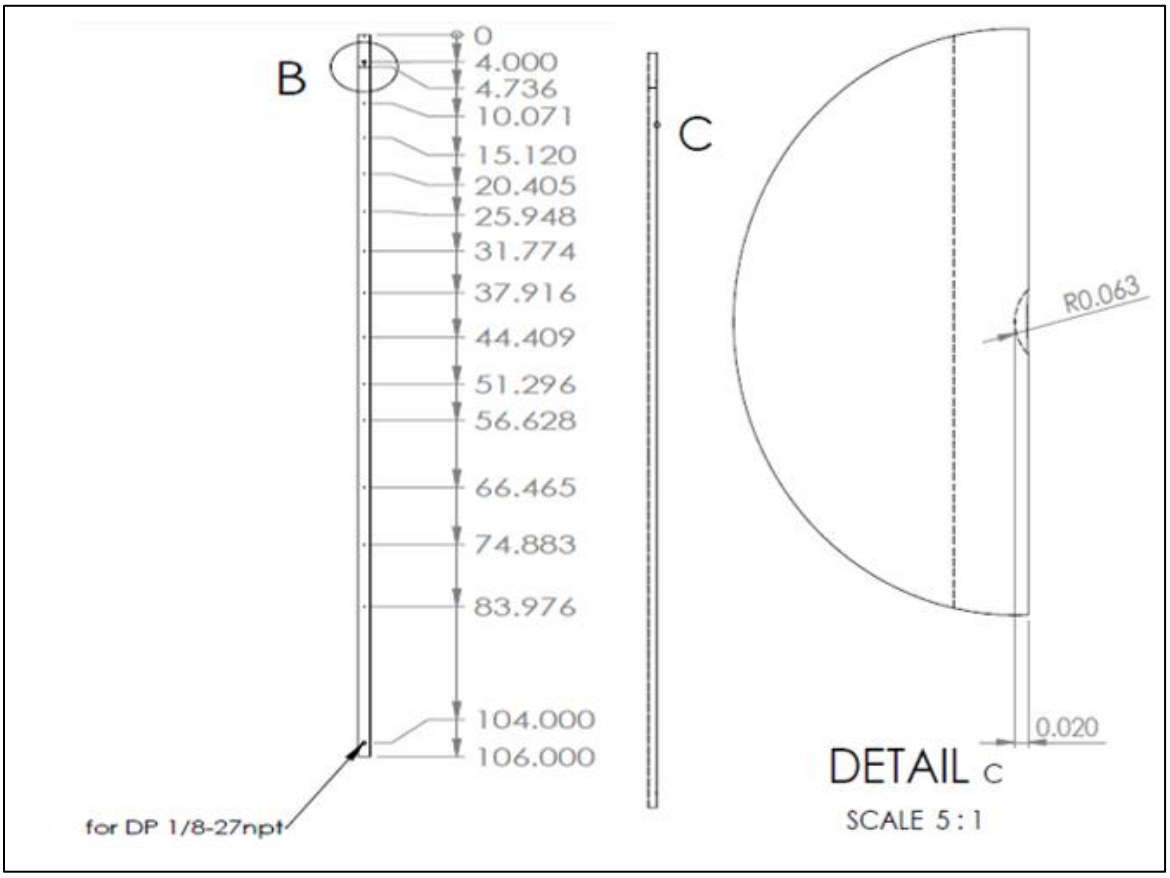

Figure 3.4 Thermistor locations on the condenser tube

4. DATA REDUCTION

The energy balance equation is used to determine local heat flux using the relation given by Equation (24).

$$q"_{wi}(z) = -\frac{w_c\, c_p}{\pi\, d_i}\frac{dT_{b,c}(z)}{dz} \tag{24}$$

$T_{b,c}$ is the axial distribution of bulk coolant temperature and is to be calculated using the CFD analysis conducted using the $k-\varepsilon$ turbulence model. This is done to obtain the temperature profile factors (F) as shown in Equation (25).

$$F = \frac{T_{wo}-T_{b,c}}{T_{wo}-T_a} \tag{25}$$

T_{wo} and T_a represent the annulus inner and outer wall temperatures respectively. They act as boundary conditions for determining the axial distribution of bulk coolant temperatures. Due to strong mixing because of turbulent flow, the variable boundary condition is expected to have only a small effect on the *F* value. As the data pertaining to only fully developed flow will be reported, this method is expected to give a good prediction of the axial bulk temperature distribution. [17]

Equation (26) can be used to calculate the experimental heat transfer coefficient

$$h_{exp} = \frac{q"_{wi}}{T_b^s - T_{wi}} \tag{26}$$

T_b^s represents the local bulk saturation temperature and T_{wi} indicates the inner wall temperature of condenser tube. T_b^s can be evaluated by subtracting the bulk non-condensable gas mass fraction from the inlet vapor flow rate. [17]

The laminar film thickness is found by the theoretical hydrodynamic analysis of falling film. [17] Equation (27) gives the condensate film flow rate per unit perimeter.

$$\Gamma = \frac{g}{\mu}\rho_1(\rho_1-\rho_m)\frac{\delta_f^3}{3} + \frac{\rho_1\tau_i\delta_f^2}{2\mu_1} \tag{27}$$

Equation 28 can be used to find the interfacial shear stress, τ_i, by considering the suction effect of condensation phenomena.

$$\tau_i = 0.5 f_{io} \rho_m (u_m - u_i)^2 \frac{\beta_f}{\exp(\beta_f) - 1} \tag{28}$$

Where u_m represents the velocity of bulk steam-gas mix, u_i signifies the interface velocity, and β_f is the blowing parameter. [34]

$$\beta_f = \frac{m''}{\rho_m u_m f_{io}/2} \tag{29}$$

Where m'' has a negative value of condensation mass flux.

From Equation (23), laminar film thickness at $\tau_i = 0$ reduces to Nusselt's analysis [32] which is given by

$$\delta_{fo} = \left(\frac{3 u_1 \Gamma}{g \rho_1 (\rho_1 - \rho_m)}\right)^{1/3} \tag{30}$$

Eq. (27) can be converted to a dimensionless form Eq. (30) by using dimensionless parameters $Re_f = \Gamma / u_1$, $\delta_f^* = \delta_f / L$, $\tau_i^* = \tau_i / (\rho g l)$, $L = (v_1^2 / g)^{1/3}$

$$\frac{Re_f}{1 - (\rho_m / \rho_1)} = \frac{\delta_f^{*3}}{3} + \frac{\tau_i^* \delta_f^{*2}}{2} \tag{31}$$

The theoretical value of film Nusselt number using characteristic length L is obtained by Equation 32.

$$Nu = \frac{h_f L}{k_1} = \frac{1}{\delta_f^*} \tag{32}$$

5. STAR-CCM+ CFD CODE VALIDATION

5.1. GEOMETRY

The geometry model for CFD simulations represented a simple concentric tube heat exchanger. Three models with different pipe diameters were created for the purpose of CFD analysis. All geometries were first created in SOLIDWORKS 2014 and saved as .x_b extension files. These files were later imported into STAR-CCM+ version 11.02.009 for CFD analysis. As shown in Figure 5.1, the modeled geometry was a cylindrical concentric pipe system which was sliced along the condenser tube axis to obtain a circumferentially symmetric configuration. This was done to reduce both the computational resources and total time required for simulation.

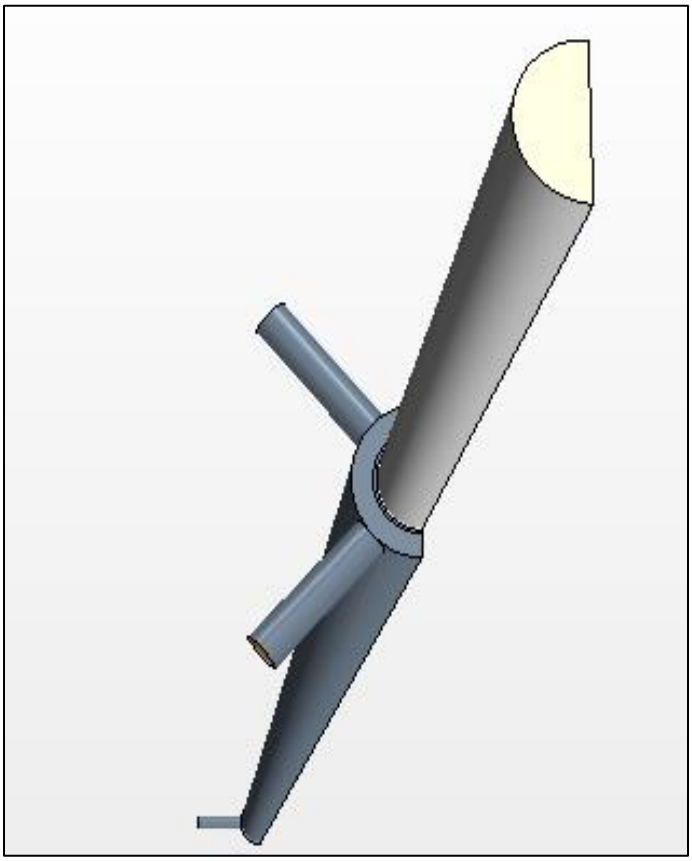

Figure 5.1 SolidWorks 3D model of the test section.

The first 3D model was created to validate STARCCM+ condensation modelling by simulating Kuhn's experimental conditions. Therefore, the geometrical components of this model were based on Kuhn's test section. The 3D CAD included a 2.56 meter long steel tube of 2 inch outer diameter and a 1.68 mm thick pipe wall. A 2.4 meter long geometry was made on the outer side of the steel tube to model cooling water. The outer diameter of water jacket corresponded to the inner dimensions of a 3 inch schedule 80 pipe. This 3 inch pipe was used as an adiabatic steel jacket in Kuhn's [21] , [17] experiments but was not modeled in this CFD study. It is important to note that the absence of the steel water jacket will not affect the simulations results due to its adiabatic nature. Steam/vapor mixture is modeled on the inside of the steel tube. As seen from the Figure 5.2, the steam was divided into an adiabatic upstream region of length equal to 10 pipe diameters and a 2.56 meter long downstream region. The upstream adiabatic region is where flow development takes place while the CFD analysis of heat transfer is performed only in the downstream region.

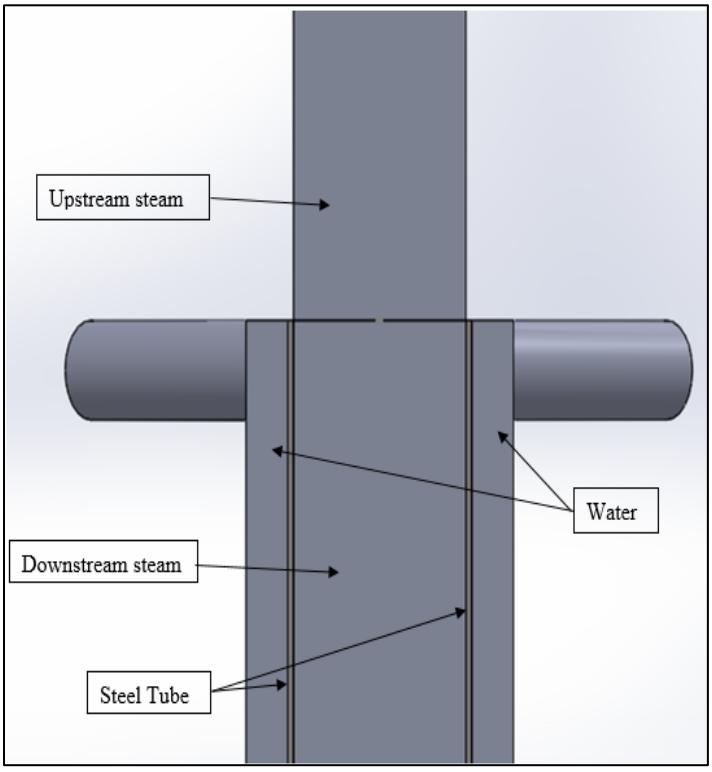

Figure 5.2 STAR-CCM+ geometry parts

The other two geometric models included a 1 inch and a 4 inch steam/vapor section. The geometric details of all three test sections can be seen in the Table 5.1.

Table 5.1 Dimensions of 3D geometries created for simulation

	Steam/Vapor Diameter (inches)	Steel tube Diameter & Thickness (inches)	Water Outer Diameter(inches)
Geometry 1	1.097”	OD=1.315”; Thickness=.109”	2.067”
Geometry 2	1.87”	OD=2”; Thickness=0.0649”	2.90”
Geometry 3	4.260”	OD=4.5”; Thickness=.120	6.065”

5.2. MESHING

Meshing is an integral part of a CFD simulation. It is important to have correctly formed mesh with optimum number of cells to analyze the physical interactions taking place in a CFD simulation. The parts of computational domain imported from SOLIDWORKS was assigned to regions and a 3D volume mesh was created using the region based meshing approach of STAR-CCM+. Figure 5.3 shows the continuum models that were selected for the purpose of meshing.

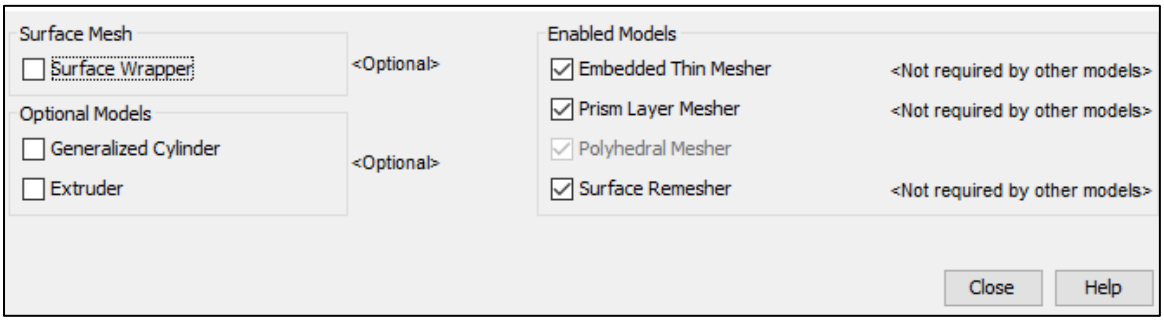

Figure 5.3 Selected models for meshing.

All the regions including upstream steam, downstream steam, steel tube and water were assigned to the same mesh continua. This was essential in order to achieve a conformal match at the interfacial nodes between steam-steel interface and steel-water

interface. During the CFD simulations, interfaces play a key role in transfer of mass, momentum and energy from one region to another.

The Prism Layer meshes are responsible for capturing the near wall behavior, while Polyhedral meshes were used to model the bulk steam and water regions. Steel tube was modeled by the Embedded Thin Layer and the Surface Remesher was used to refine the surface mesh quality and optimize it for the volumetric meshing models.

All interfaces were checked for conformal match which ensured proper connectivity of node to nodes. This is an important property for conjugate heat transfer that will take place in the CFD analysis. Figure 5.4 represents a cross sectional view of a characteristic mesh created on all regions. A mesh optimization study was performed on the steam side to get the most optimum mesh size for mesh independence. Table 5.2 summarizes the parameters for mesh convergence study.

Table 5.2 Mesh comparison parameters

Mesh	Base size(inches)	Number of Nodes	Wall y+	Film thickness at outlet (mm)
Mesh 1	1.35	6.79E+04	2.97	0.117
Mesh 2	0.9	1.39E+05	2.042	0.125
Mesh 3	0.6	3.66E+05	1.41	0.1301
Mesh 4	0.4	5.80E+05	0.92	0.13269
Mesh 5	0.2667	1.63E+06	0.579	0.1354
Mesh 6	0.1778	3.42E+06	0.3922	0.138

Each mesh base size was reduced by 2/3rd of the previous base size and a total of six meshes were compared by plotting steam centerline temperatures and the film thickness versus the number of nodes as shown by Figures 5.5 and 5.6. For this study, an extrapolated temperature boundary condition was used at the outer wall of steel tube. The temperature data was taken form Kuhn's experimental results of 2.1-8R run [21]. The maximum prism layer thickness was kept as 10% of the base size. This property influences the wall y+ values of the simulation. It is important to keep the wall y+ value lower than 1 to capture the viscous sublayer behavior. From the Table 5.2, meshes 4 to 6 have a y+ of lower than 1 which implies that the mesh is fine near the steel tube walls to capture the viscous sublayer behavior. Figure 5.5 shows a converging trend in the

condensate film thickness at the pipe outlet as the number of nodes increase. This gives a measure of the latent heat transfer from bulk steam to the condensate film for different mesh sizes.

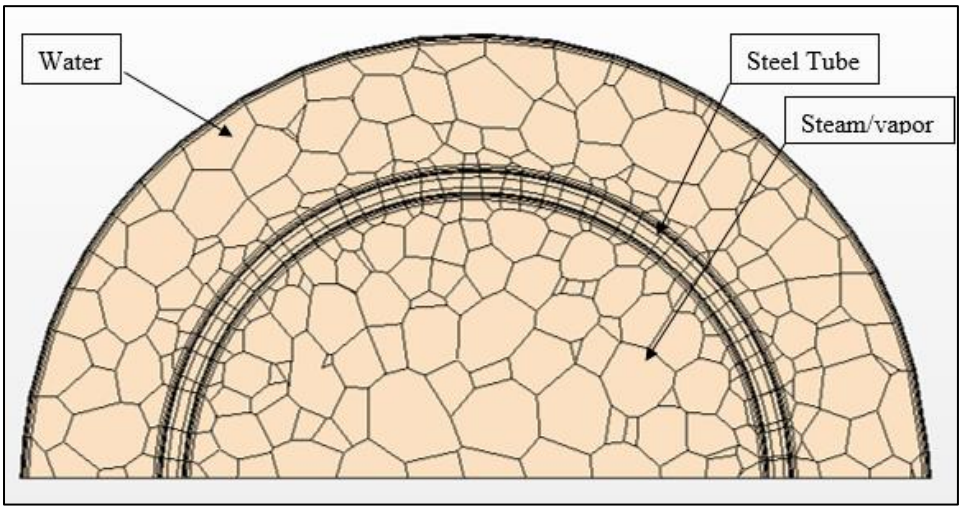

Figure 5.4 Cross sectional view of a characteristic mesh

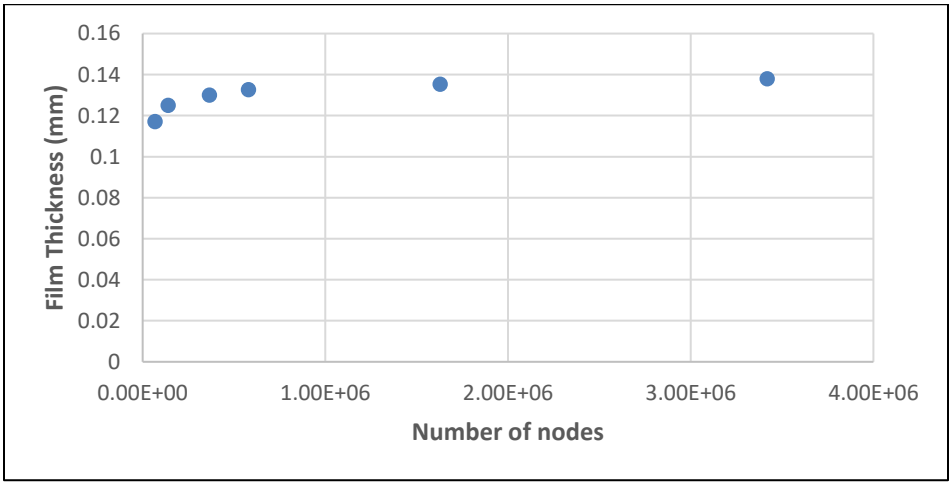

Figure 5.5 Condensate film thickness vs number of nodes

Figure 5.6 shows a plot of the centerline temperatures of steam/vapor mix versus the axial location. The temperature profile for various mesh sizes is plotted along with the results from Kuhn's results for the run 2.1-8R [21]. It can be concluded that Mesh 5 represents convergence for this mesh study in terms of both condensate film thickness

and centerline temperature distribution. Also, the y+ value of 0.579 for Mesh 5 agreeably captures the near wall effects. Therefore Mesh 5, with the base size of 0.266 inches, will be adopted for further CFD analysis in this study.

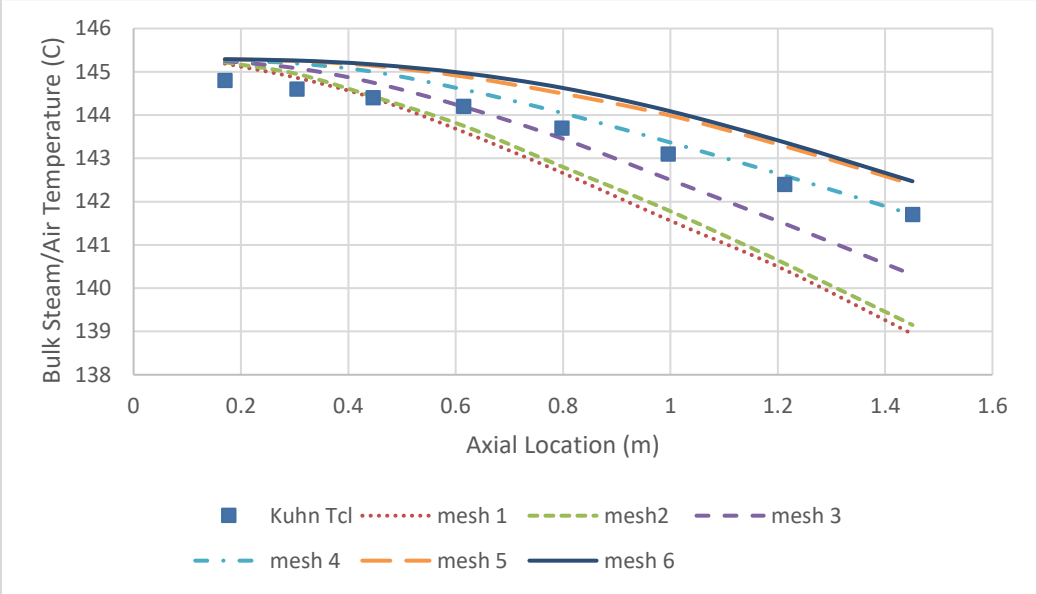

Figure 5.6 Bulk temperature distribution for different mesh sizes

5.3. PHYSICS MODELS

Based on the literature studies and the experimental conditions, the most applicable physics models were chosen to represent the different regions of the CFD simulation. Table 5.3 summarizes all the physics conditions used to model Steam/vapor, steel tube and water regions. The CFD simulation was modeled as an implicit and unsteady as this behavior is inherent to the condensation model applied in STARCCM+.

The steam/vapor is modeled as a multi-component gas. This facilitated the addition of a non-condensable gas phase along with the basic steam phase. A multiphase interaction model was switched on along with a fluid film model. The connectivity of steam with the liquid condensate phase was set up to model the condensation behavior. Furthermore, an implicit coupling of thermal and hydrodynamic effects was enabled to model condensation close to saturation temperatures. Due to the turbulent nature of both the steam and water, the realizable $k-\in$ model was used to represent the physics.

Table 5.3 Physics models used to represent different regions

Steam/Vapor Physics	Water Physics	Steel Tube Physics
• Three dimensional • Implicit Unsteady • Multi-component Gas • Non-Reacting • Segregated Flow • Gradients • Segregated Species • Turbulent • Reynolds-Averaged Navier Stokes • K-Epsilon Turbulence • Realizable K-Epsilon two-layer • Exact Wall Distance • Two Layer All Y+ Wall Treatment • Gravity • Segregated Fluid Temperature • Ideal Gas • Fluid Film • Multiphase Interaction	• Three dimensional • Implicit Unsteady • Liquid • Segregated Flow • Gradients • IAPWS-IF97(Water) • Segregated Fluid Temperature • Turbulent • Reynolds-Averaged Navier Stokes • K-Epsilon Turbulence • EB K-Epsilon • Exact Wall Distance • EB K-Epsilon All Y+ Wall Treatment • Gravity	• Three dimensional • Implicit Unsteady • Solid • Segregated Solid Energy • Gradients • Constant Density

For the liquid film model to be applicable, a shell region was created out of the interface connecting the steam to steel tube. The physics applicable to the liquid condensate phase was then allocated to this newly created region. All the material properties of water, steam and condensate needed to be fixed according to the reference pressures and temperatures before proceeding to the setting up of boundary conditions.

5.4. SIMULATION PROCEDURE

CFD simulations were performed by two distinct methods for STAR-CCM+ code validation. The first method involved simulating a simplified iterative approach in which the water side and steam side were modeled individually. For the second method, both water and steam were modeled in one CFD simulation by fixing the boundary conditions at the water and steam inlets according to Kuhn's [21] experimental data.

For the first case, a linear temperature profile of 20 to 80 degrees Celsius was used as an initial guess as a boundary condition at the outside condenser tube (steel tube) walls and the steam/vapor side was simulated. From the results of this simulation, the temperature data at the inside wall of steel tube was extracted and used as a boundary condition for running the CFD case of water side. This process was repeated until the results at each side converged in terms of temperature distributions.

For the simulations done on Geometry2, as shown in Table 5.1, the mass flux of water and steam along with the operating inlet temperatures and pressure was fixed according to Kuhn's experimental data. For the Geometry1 and Geometry3, the inlet velocities of both water and steam side were scaled according to the pipe diameters. Due to the dependence of experimental Heat Transfer Coefficient on the Reynolds Number as shown in Table2.1, the inlet Reynolds number was kept as constant for scaling the inlet velocities of steam/vapor mix and water for both Geometries 1 and 3.

5.5. SIMULATION RESULTS

5.5.1. Seed Density Variation Study. As noted in the Section 2.2.1, the droplet seed density (N_seeds) is a parameter used by STARCCM+ to simulate condensation on dry walls. As it is difficult to quantify this parameter experimentally, there is no data available data for the best suited value of this parameter. A study was therefore performed to find the best value of N_seeds that will give acceptable results. The steam side of the Geometry2 was simulated for the purpose of this study. The input parameters for this study were taken from Kuhn's test run 2.1-8R and are summarized in the Table 5.4. The outside wall of steam was set as a constant temperature boundary. A 3rd order polynomial function was used to fit the data from Kuhn's outer wall Temperature (T_{wo}).

This function was then used to extrapolate the temperature profile at various axial locations for the outside steel wall.

Table 5.4 Kuhn's 2.1-8R Experimental Run conditions.

Inlet Pressure	413100 Pa
Steam/Air Inlet Temperature	145.3^{o}C
Steam Mass Flow Rate	51.2 kg/hr
Mass Flow Rate of Air	8.87 kg/hr
Mass Flow Rate of Water	925.1kg/hr
Water Inlet Temperaure	27.5 ^{o}C

From the seed variation study, it was seen that the simulation tended to diverge for a zero droplet seed density. The study was performed for the seed density varying from 1 (m4.1) to 10000 (m4.7) seeds per square meter. Figure 5.7 shows the plot of the variation in the centerline temperature of the bulk steam-air mixture against the axial distance. It was found that the best results were obtained from a seed density of 1000 droplets per square meter. Each simulation was performed for a total physical time of 15 minutes which was enough for the residuals to converge and stabilize thus indicating steady state behavior. The temperature profiles for lower seed densities decrease at a higher rate along the length of the condenser pipe. This indicates a higher prediction of sensible heat transfer and a lower condensation rate. It can be observed from Figure 5.5 that m4.5 gives a centerline profile which is nearly parallel to Kuhn's experimental measurements. It can therefore be inferred that this profile gives the best possible estimates for prediction of condensation.

To check the independence of seed variation study on the input parameters, another simulation run was performed. Experimental data from Kuhn's Test Run 1.1-1 was used for setting up the simulation. Unlike the previous simulation, this was a pure steam case. It was seen that droplet seed density of 1000 seeds per square meter predicted the centerline temperature well for this case. The details of input parameters for this case and the plot of bulk steam temperature distribution can be found in Appendix A for further reference.

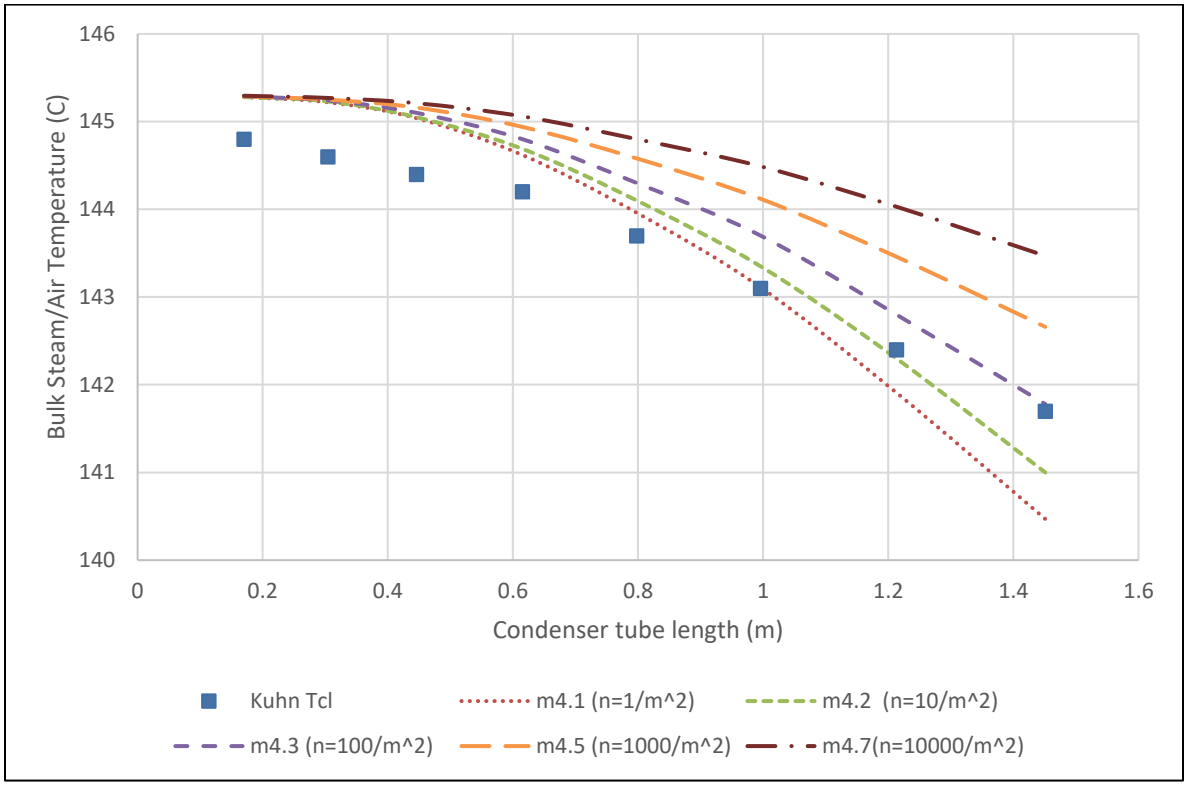

Figure 5.7 Droplet seed density variation study

5.5.2. Validation of Physics Models. To check the applied physics for both water and steam/vapor region, CFD simulations were performed on individual regions. The steam side was simulated along with the condenser steel tube for 2different cases. The outer cylindrical wall temperatures were fixed according to the extrapolated temperature data obtained from Kuhn's experimental run 1.1-1 for first case and run 2.1-8R for the second case. A third order polynomial was used to extrapolate the temperatures from the set of 8 measurements provided by Kuhn's study. Figures 5.8 and 5.9 show the comparison of experimental and CFD bulk temperature distribution at various axial location. It can be seen that the CFD results closely follow the experimental results thus justifying the validity of the physics models used for the steam region in CFD simulation.

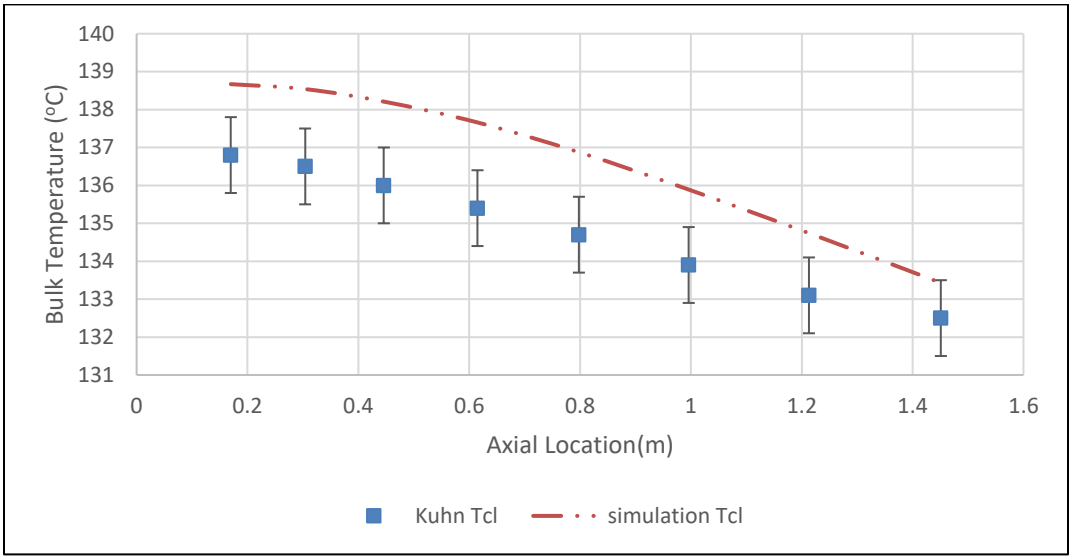

Figure 5.8 Bulk temperatures for Kuhn1.1-1 run on steam region

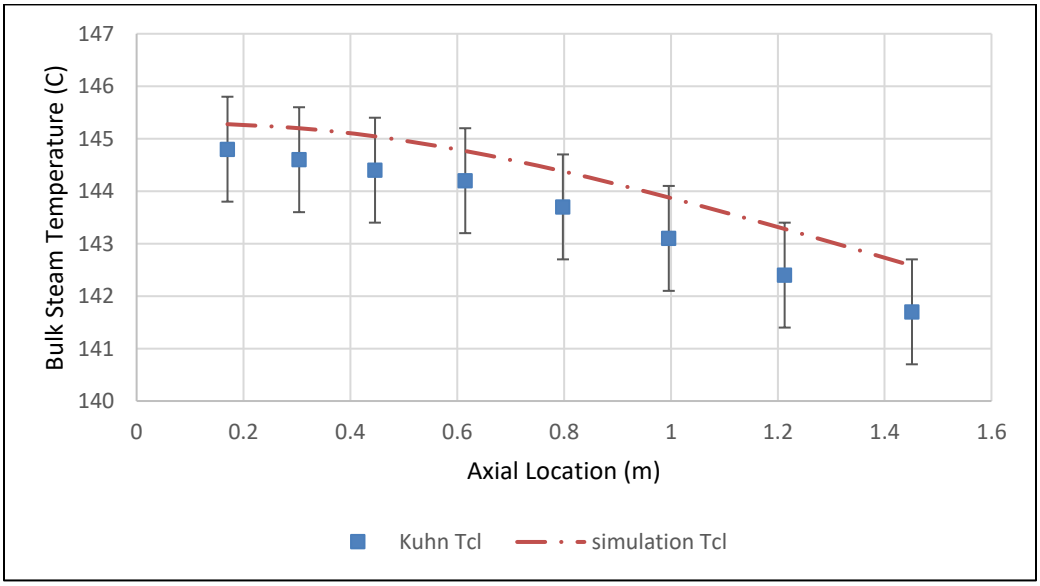

Figure 5.9 Bulk temperatures for Kuhn2.1-8R run on steam region

For validating the water side physics, the water region was simulated along with the steel tube and the temperatures of the inside wall of condenser tube were extrapolated from the experimental data. Simulations were performed and compared only with Kuhn's results from run1.1-1. As the operating pressure of water side will remain the same for all cases, comparison with one run was sufficient to establish the validity of chosen physics

models to represent this region. Figure 5.10 shows the temperature distribution of outside adiabatic wall of water for experimental and CFD simulations. It can be seen that the CFD prediction temperatures closely follow the experimental results. Therefore, the physics models used to represent the steam/vapor and water regions are reasonably well set up for use in further CFD analysis.

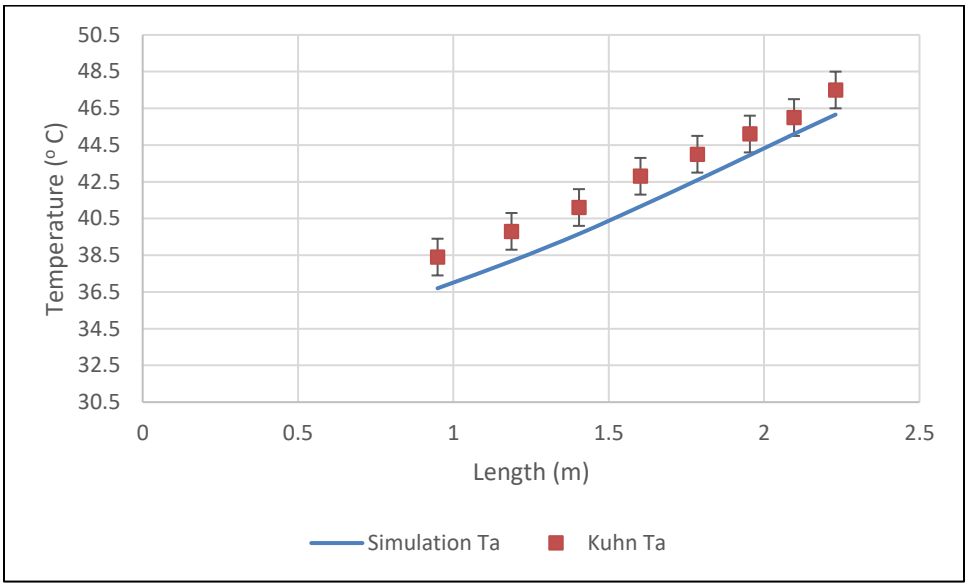

Figure 5.10 Adiabatic wall temperatures for Kuhn1.1-1 run on water region

5.5.3. Iterative Study Results. This was a simplistic approach adopted to perform CFD simulations. The iteration process was started by fixing the temperature boundary condition at the outside was of the steel tube. A linear temperature profile of 20 to 80degree Celsius, was adopted. This assumption was backed the fact that during the experiments, the water side would see a temperature increase from 20^{o}C at inlet to 80^{o}C at the exit of test section. The steam side was first simulated and the results of this simulation were used to plot a temperature distribution at the inside wall of steel tube. This was used as a boundary condition, representing steam/steel wall interface temperatures in CFD simulations of water side. Figure 5.11 shows the individual geometries used to represent steam-steel tube and water-steel tube regions for the CFD study.

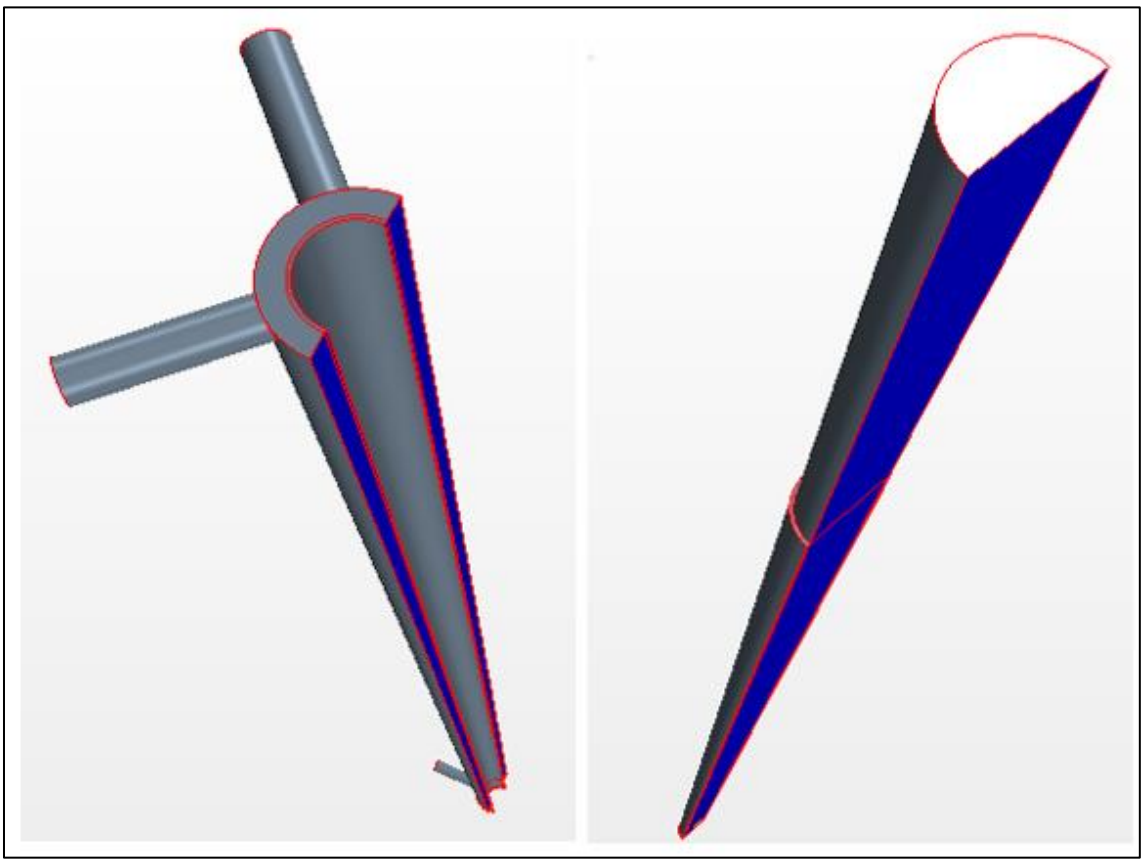

Figure 5.11 Individual geometries used in Iterative Study

The outside wall temperatures for water and the bulk/centerline temperature for steam/vapor mix were plotted to observe the convergence of results. It was seen that the convergence was achieved in 5 iterations for the water side. However, for the steam side, a negligible variation in the bulk temperatures was seen from one iteration to another. Figures 5.12 and 5.13 show the results from iterative study on the 2 inch test section. The steam bulk temperatures are shown by fs1 to fs1.4 in Figure 5.9. and it can be noted that the temperature profiles overlap each other. The error bars shown represent the error from Kuhn's experimental measurements. It can be concluded that the CFD results for bulk temperatures agreed with the experimental data for the steam side.

Fw1 to fw1.4 in Figure 5.13 show the temperatures profiles at water outer diameter. It was seen that the simulation results under predict the temperature rise in the water region. This implies that the simulation under predicts the total heat transferred to the water.

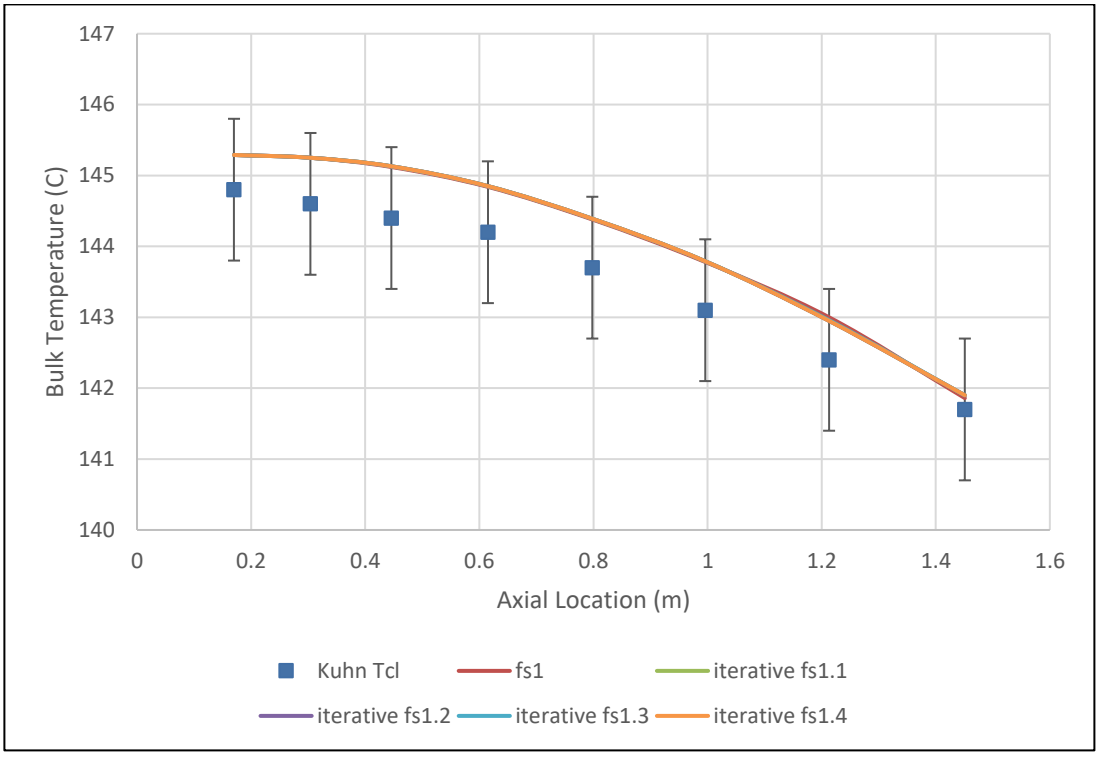

Figure 5.12 Iterative study results for steam

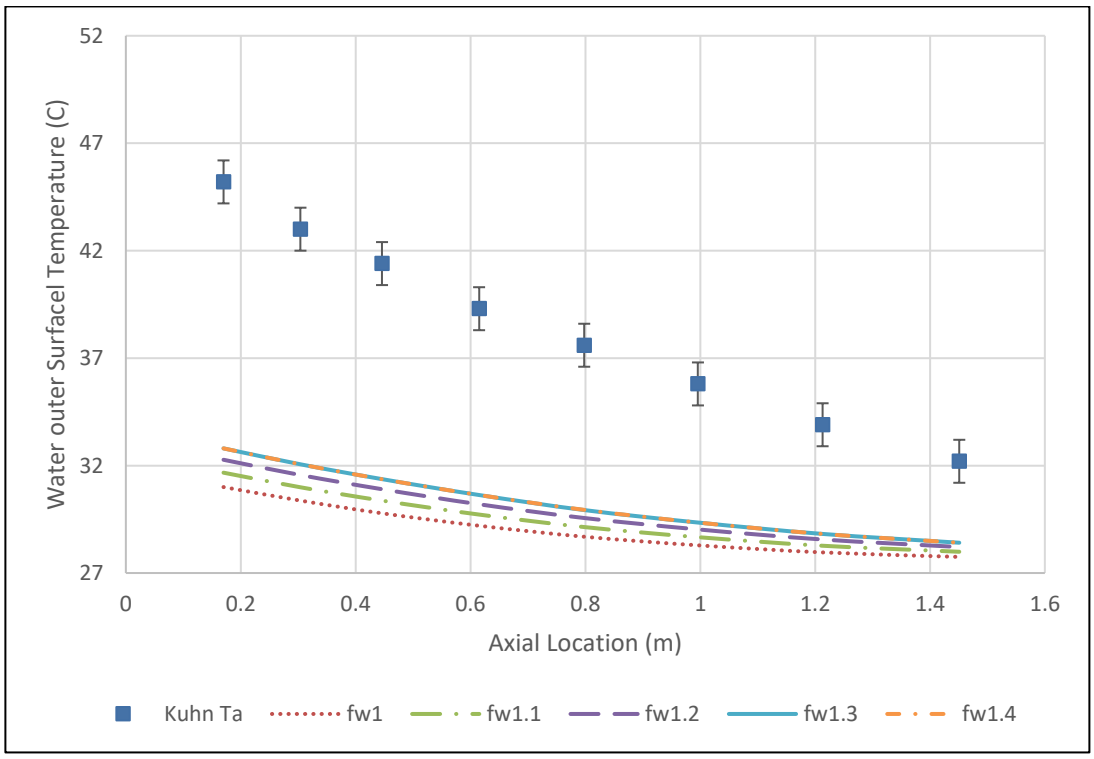

Figure 5.13 Iterative study results for water

5.5.4. Combined Study Results. For all the 3 geometries, simulations were performed at an inlet pressure of 413100Pa and with 14.8% air mass fraction, in accordance with Kuhn's 2.1-8R test run. The mass flow rates of both the water and steam-air mixture for the geometry 2 were kept same as the experimental inlet conditions. Figure 5.14 shows the plot of Kuhn's centerline temperature (T_{cl}), outside condenser-wall temperature (T_{wo}) and adiabatic water wall temperature (T_a) with the respective results from the CFD study on geometry 2. Kuhn's measurements were given at 8 axial locations for all the temperatures while CFD study gives a much higher resolution with outputs on each node. It can be seen that the centerline temperatures for both experiment and CFD study are very close to each other however, the CFD simulation under predicts the outside wall temperatures of condenser tube and water. This implies a lower heat transfer coefficient prediction by the CFD study, leading to smaller heat transfer to the water. Table 5.5 summarizes the absolute error for CFD temperature predictions of the Geometry 2 at various axial locations for all 3 temperature profiles.

Table 5.5 Absolute error in STARCCM+ temperature predictions

axial location (m)	% Error in T_{cl}	% Error in T_{wo}	% Error in T_a
0.17	0.3446	11.6730	17.9646
0.304	0.4730	11.5490	15.6279
0.446	0.5720	9.96957	14.4927
0.615	0.5846	11.688	12.417
0.798	0.6889	11.6221	11.25
0.996	0.7407	9.5744	9.8603
1.213	0.716	6.3	7.8171
1.451	0.5850	2.2273	5.900

Figure 5.15 represents a comparison of Heat Transfer Coefficients (HTCs) from the simulations and the experiments. The calculation of HTC from STARCCM+ was done based on the difference between the bulk saturation temperature and the inside wall temperature of the condenser tube obtained from the CFD results. Heat transfer coefficients at each axial location were obtained by dividing the local boundary heat flux

at the condensate-condenser tube interface with the obtained temperature difference. Local mole fraction of water at various axial locations was used to calculate the local bulk saturation temperature. Appendix C can be referred for further information on HTC calculation. From Figure 5.15, it can be seen that the CFD simulation under-predicts the HTC. This implies that the STARCCM+ code does not capture the complete physical phenomena of condensation heat transfer with the inbuilt codes.

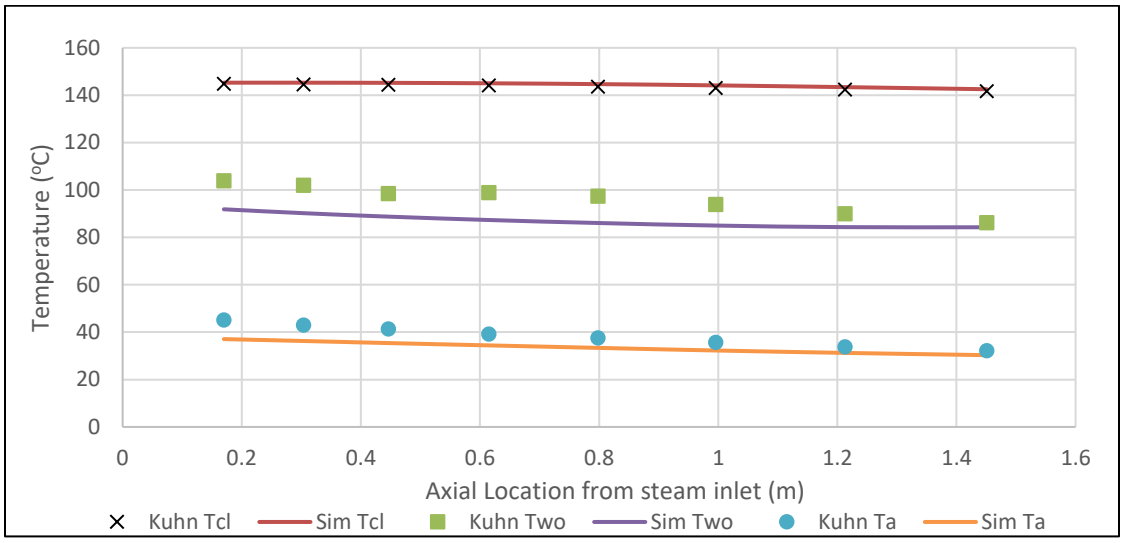

Figure 5.14 CFD results vs simulation results for Geometry 2

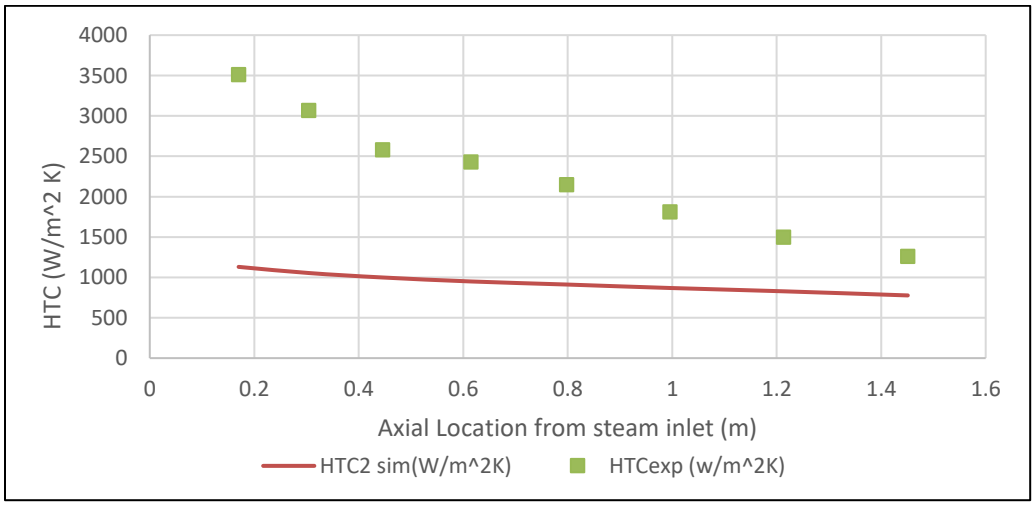

Figure 5.15 HTC comparison between CFD and experiment

Table 5.6 summarizes the absolute error of CFD heat transfer coefficient for Geometry 2 at various axial locations. It can be seen that the HTC predicted by STARCCM+ near the steam inlet is nearly 68% of that of experimental value. As the axial location increases, this error tends to reduce along with the length. However, an error of 38% near the 1.5meter downstream location signifies that there is a substantial discrepancy between the predicted and the experimental heat transfer coefficients.

Table 5.6 Error in CFD HTC relative to experimental results

Axial location (m)	% Error in HTC
0.17	67.801
0.304	65.664
0.446	61.284
0.615	60.920
0.798	57.607
0.996	52.014
1.213	44.811
1.451	38.381

Simulations were also performed on the Geometry1 and Geometry3 at the reference pressure of 413100Pa with the properly scaled inlet velocities. In order to check the effectiveness of CFD results for scaling the condensation heat transfer, a study was performed to compare Heat transfer coefficients from all 3 geometries. According to Kuhn's relation, there was no indicated diameter dependence of heat transfer coefficient. This was attributed to an improper non-dimensionalization of the shear stress term represented by Equation 28.

As mentioned in Table2.1, Equation 32 gives the correlation developed by Lee and Kim [18] for the prediction of condensation heat transfer. From the Equation 33 and 34, it was seen that the experimental mixture heat transfer coefficient is dependent on the diameter as $d^{-0.6248}$.

$$f_{mix} = \frac{h_{exp,mix}}{h_{Nu}} = \tau^{*0.3124}_{mix} \left(1 - 0.964 W_{nc}^{0.402}\right) \tag{32}$$

$$\tau^* = \frac{\frac{1}{2}\rho_{mix} u_{mix}^2 f}{g\rho_f L} \quad (33)$$

$$u_{mix} = Re_{mix}\mu_{mix}/\rho_{mix} d \quad (34)$$

f denotes the friction factor which is based on the mixture Reynolds number Re_{mix}.The mixture density is denoted by ρ_{mix} and d is the pipe diameter.

Table 5.7 gives the expected diameter ratio dependence of heat transfer coefficient relative to the condenser tube diameter of Geometry 1. It was seen that as the diameter of steam/vapor region increased form Geometry1 to Geometry3, the HTC ratio calculated from STARCCM+ results decreased. Using the diameter dependence of the heat transfer coefficient, predicted values of STAR-CCM+ can be scaled as shown in the Table 5.8. Although, the result shown in Table 5.8 captures this behavior to some extent, the discrepancies from the predictions of Lee and Kim's [18] correlation need to be addressed.

Table 5.7 Expected diameter ratio dependence of HTC

Diameter ratio
$(d_1/d_1)^{-0.6248}$ =1
$(d_2/d_1)^{-0.6248}$ =0.716
$(d_3/d_1)^{-0.6248}$ =0.428

Table 5.8 Scaling analysis of Heat Transfer Coefficient

Axial Distance (m)	0.17	0.304	0.446	0.615	0.798	0.996	1.213	1.451
HTC Ratio Geometry2/1	0.884	0.883	0.877	0.877	0.876	0.868	0.865	0.852
HTC Ratio for Geometry3/1	0.709	0.69	0.673	0.661	0.643	0.622	0.609	0.599

6. CONCLUSION AND FUTURE WORK

A validation study was performed to evaluate the capability of STARCCM+ to predict the condensation heat transfer coefficient. Three geometries, with progressively increasing pipe diameters were analyzed to look at the scaling competence of the software. Simulations were performed by 2 different methods. First was an iterative study to individually simulate either region. The second method was a combined simulation of both water and steam/vapor region with conjugate heat transfer between them.

It was observed that for both the iterative and combined study, the software acceptably predicts the general trends of temperature distribution at various axial and radial locations. A maximum error of 18% was found in the predictions of water adiabatic wall temperatures. The error percentage reduced along with the axial location to a minimum of 5.9% at 1.45 meter location from steam inlet. Errors in the prediction of heat transfer coefficient were much more significant as they ranged from 68% near the inlet to 38% at 1.45 meters downstream of steam inlet. This can be attributed to the heat flux calculation method adopted by the software.

It can be concluded that the software needs to account for additional physical behavior in the existing models for acceptably predicting the results of heat transfer in condensation phenomena. Consequently, there is a need to improve the inbuilt code for the prediction of condensation heat transfer in STAR-CCM+.

A test section was designed and fabricated based on the 1 inch condenser tube geometry. The future work will involve running experiments on this test section at temperatures ranging from 100 ºC to 165 ºC and pressures up to 100 psia. Two more test sections with condenser tube diameters of 2” & 4” will be fabricated and used for experimentation. The condensation heat transfer rate with and without the presence of non-condensable gases will be measured and the results will be compared with the existing models to perform a scaling analysis.

APPENDIX A

KUHN'S DATA AND SEED VARIATION STUDY RESULTS

KUHN'S RUN 1.1-1 [21]

Inlet Pressure	113900 Pa
Steam/Air Inlet Temperature	138.8°C
Steam Mass Flow Rate	60.2 kg/hr
Mass Flow Rate of Air	0 kg/hr
Mass Flow Rate of Water	999.8kg/hr
Water Inlet Temperaure	31.5 °C

SEED VARIATION RESULTS BASED ON KUHN 1.1-1 RUN

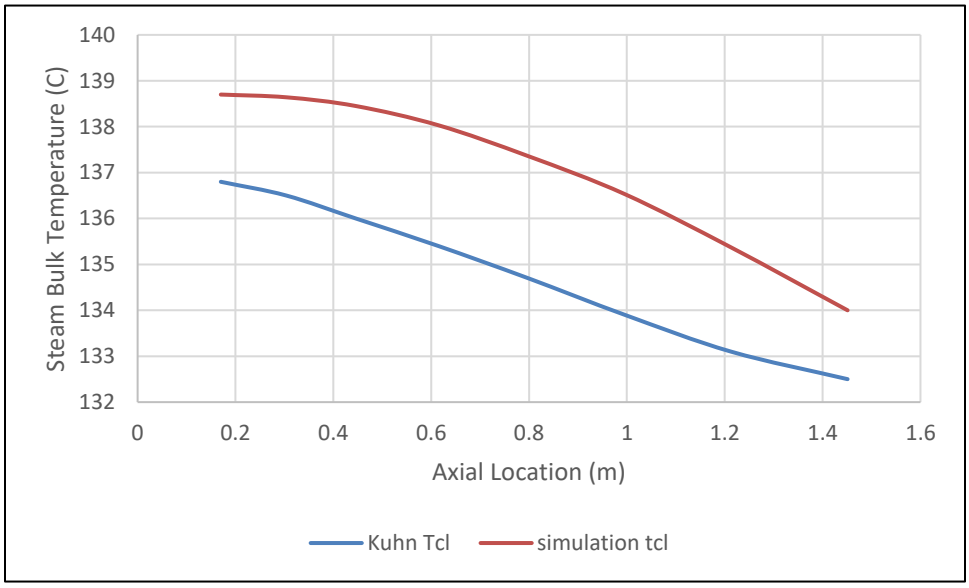

APPENDIX B

ITTERATIVE STUDY RESULTS FOR 2INCH TEST SECTION

STEAM SIDE RESULTS

Simulation location (m)	Kun's Location (m)	Kuhn Tcl (°C)	fs1 (°C)	iterative fs1.1 (°C)	iterative fs1.2 (°C)	iterative fs1.3 (°C)	iterative fs1.4 (°C)
2.23	0.17	144.8	145.29	145.29	145.29	145.29	145.29
2.096	0.304	144.6	145.25	145.25	145.25	145.25	145.25
1.954	0.446	144.4	145.12	145.13	145.13	145.13	145.13
1.785	0.615	144.2	144.84	144.85	144.85	144.85	144.85
1.602	0.798	143.7	144.38	144.39	144.39	144.39	144.39
1.404	0.996	143.1	143.78	143.79	143.79	143.79	143.79
1.187	1.213	142.4	143	142.95	142.95	142.96	142.95
0.949	1.451	141.7	141.86	141.9	141.9	141.9	141.9

WATER SIDE RESULTS

Simulation location (m)	Kuhn's Location(m)	Kuhn Ta (°C)	fw1 (°C)	fw1.1 (°C)	fw1.2 (°C)	fw1.3 (°C)	fw1.4 (°C)
2.23	0.17	45.2	31	31.67	32.27	32.8	32.8
2.096	0.304	43	30.37	30.99	31.56	32.06	32.06
1.954	0.446	41.4	29.78	30.37	30.9	31.37	31.37
1.785	0.615	39.3	29.2	29.72	30.2	30.63	30.63
1.602	0.798	37.6	28.69	29.14	29.56	29.93	29.94
1.404	0.996	35.8	28.29	28.67	29.03	29.35	29.35
1.187	1.213	33.9	27.96	28.27	28.56	28.82	28.82
0.949	1.451	32.2	27.75	27.99	28.21	28.41	28.41

APPENDIX C
HEAT TRANSFER COEFFICIENTS FOR CFD SIMULATIONS

SIMULATION RUN CONDITIONS (KUHN RUN 2.1-8R)

Inlet Pressure	413100 Pa
Steam/Air Inlet Temperature	145.3^{o}C
Steam Mass Flow Rate	51.2 kg/hr
Mass Flow Rate of Air	8.87 kg/hr
Mass Flow Rate of Water	925.1kg/hr
Water Inlet Temperaure	27.5 ^{o}C

EXPERIMENTAL HTC FOR KUHN'S RUN 2.1-8R

Kuhn's axial location (m)	HTCexp (w/m^2K)
0.17	3510
0.304	3070
0.446	2580
0.615	2430
0.798	2150
0.996	1810
1.213	1500
1.451	1260

HTC CALCULATION FOR COMBINED CFD STUDY OF GEOMETRY1

kuhn location (m)	Sim location (m)	q (w/m^2)	steam mole fraction	Psb (pa)	Tsb	Twi	HTC1 sim(W/m^2K)
0.17	2.547	54635.5	0.90269	372901.2	141.1	98.34	1277.725
0.304	2.413	53305.8	0.902	372616.2	141.07	96.39	1193.057
0.446	2.271	52735.8	0.9007	372079.2	141.02	94.7	1138.51
0.615	2.102	51793	0.8981	371005.1	140.92	93.05	1081.951
0.798	1.919	51264	0.89455	369538.6	140.77	91.45	1039.416
0.996	1.721	50973	0.89016	367725.1	140.6	89.629	1000.039
1.213	1.504	50203	0.88467	365457.2	140.38	87.875	956.1566
1.451	1.266	49262	0.878	362701.8	140.12	86.024	910.6403

HTC CALCULATION FOR COMBINED CFD STUDY OF GEOMETRY2

kuhn location (m)	Sim location (m)	q (w/m^2)	steam mole fraction	Psb (pa)	Tsb	Twi	HTC2 sim(W/m^2K)
0.17	2.304	50018.7	0.90277	372934.3	141.1	96.847	1130.16
0.304	2.17	48562.1	0.90273	372921.1	141.1	95.03	1054.09
0.446	2.028	47535.3	0.90258	372855.8	141.09	93.5	998.850
0.615	1.859	46620	0.902	372616.2	141.07	91.977	949.62
0.798	1.676	45905.4	0.9007	372079.2	141.02	90.654	911.43
0.996	1.478	44706	0.89872	371261.2	140.94	89.467	868.53
1.213	1.261	43225.5	0.8954	369889.7	140.81	88.594	827.820
1.451	1.023	40644.4	0.89107	368101	140.64	88.29	776.397

HTC CALCULATION FOR COMBINED CFD STUDY OF GEOMETRY3

kuhn location (m)	Sim location (m)	q (w/m^2)	steam mole fraction	Psb (pa)	Tsb	Twi	HTC4 sim(W/m^2K)
0.17	2.307	39018	0.902777	372937.2	141.1	98.03	905.9206
0.304	2.173	37470	0.902776	372936.8	141.1	95.765	826.5137
0.446	2.031	36431	0.902772	372935.1	141.1	93.57	766.4843
0.615	1.862	35832	0.902752	372926.9	141.1	91.02	715.4952
0.798	1.679	34878	0.902685	372899.2	141.1	88.93	668.5451
0.996	1.481	33380	0.902516	372829.4	141.09	87.43	622.0649
1.213	1.264	31703	0.902168	372685.6	141.08	86.64	582.3475
1.451	1.026	29837	0.90162	372459.2	141.05	86.36	545.5659

HTC CALCULATION FOR ITERATIVE CFD STUDY OF GEOMETRY1

kuhn location (m)	Sim location (m)	q (w/m^2)	steam mole fraction	Psb (pa)	Tsb	Twi	HTC steam only sim(W/m^2K)
0.17	2.301	66615	0.9008	372120.5	141.02	80.685	1104.086
0.304	2.167	66967	0.8988	371294.3	140.94	77.686	1058.7
0.446	2.025	67430	0.8958	370055	140.82	74.4	1015.206
0.615	1.856	68040	0.8915	368278.7	140.65	70.53	970.3366
0.798	1.673	68560	0.8862	366089.2	140.44	66.31	924.8617
0.996	1.475	68430	0.8794	363280.1	140.17	61.72	872.2753
1.213	1.258	67816	0.8706	359644.9	139.81	56.46	813.6293
1.451	1.02	66418	0.8598	355183.4	139.37	50.664	748.743

HTC CALCULATION FOR ITERATIVE CFD STUDY OF GEOMETRY2

kuhn location (m)	Sim location (m)	q (w/m^2)	steam mole fraction	Psb (pa)	Tsb	Twi	HTC steam only sim(W/m^2K)
0.17	2.303	61107	0.902755	372928.1	141.1	83.7	1064.58188
0.304	2.169	60800	0.90272	372913.6	141.1	80.25	999.178307
0.446	2.027	60408	0.90249	372818.6	141.09	76.65	937.430168
0.615	1.858	60228	0.90184	372550.1	141.06	72.426	877.524259
0.798	1.675	60500	0.9003	371913.9	141	67.85	827.067669
0.996	1.477	60195	0.89775	370860.5	140.9	62.88	771.53294
1.213	1.26	59175	0.89375	369208.1	140.74	57.35	709.61746
1.451	1.022	57820	0.8881	366874.1	140.52	51.27	647.843137

HTC CALCULATION FOR ITERATIVE CFD STUDY OF GEOMETRY3

kuhn location (m)	Sim location (m)	q (w/m^2)	steam mole fraction	Psb (pa)	Tsb	Twi	HTC steam only sim(W/m^2K)
0.17	2.307	45692	0.90277	372934.3	141.1	84.63	809.1376
0.304	2.173	44164	0.90276	372930.2	141.1	81.165	736.8649
0.446	2.031	42591	0.902732	372918.6	141.1	77.64	671.1472
0.615	1.862	41606	0.90263	372876.5	141.09	73.483	615.4096
0.798	1.679	40302	0.902455	372804.2	141.09	68.865	558.0062
0.996	1.481	39132	0.902146	372676.5	141.08	64.09	508.2738
1.213	1.264	38605	0.90158	372442.7	141.05	58.835	469.5615
1.451	1.026	37575	0.90063	372050.3	141.02	53.15	427.6203

REFERENCES

[1] International Atomic Energy Agency, "From Obninsk Beyond: Nuclear Power Conference Looks to Future," 24 June 2004. [Online]. Available: https://www.iaea.org/newscenter/news/obninsk-beyond-nuclear-power-conference-looks-future. [Accessed 26 December 2015].

[2] International Atomic Energy Agency, "Power reactor information system," [Online]. Available: https://www.iaea.org/pris/. [Accessed 26 December 2015].

[3] International Atomic Energy Agency, Indicators for nuclear power development, Vienna: International Atomic Energy Agency, 2015.

[4] F. L. Toth and H.-H. Rogner, "Oil and nuclear power: Past, present, and future," *Energy Economics*, vol. 28, pp. 1-25, 2006.

[5] World Nuclear Association, "Small Nuclear Power Reactors," [Online]. Available: http://www.world-nuclear.org/information-library/nuclear-fuel-cycle/nuclear-power-reactors/small-nuclear-power-reactors.aspx. [Accessed 08 september 16].

[6] D. R. F. W. Matthew C. Smith, "Westinghouse Small Modular Reactor Passive Safety System Response to Postulated Events," in *ICAPP*, Chicago, 2012.

[7] "U.S.NRC," NuScale Power, LLC, 2014. [Online]. Available: http://www.nrc.gov/reactors/advanced/nuscale.html.

[8] L. NuScale Power, "NuScale Plant Design Overview," 2013.

[9] SMR, LLC, "SMR-160 Overview," [Online]. Available: https://smrllc.com/technology/smr-160-overview/. [Accessed 16 september 2016].

[10] Generation mPower LLC, "Generation mpower," [Online]. Available: http://www.generationmpower.com/. [Accessed 19 September 2016].

[11] D. Othmer, "THE CONDENSATION OF STEAM," *Industrial and engineering chemistry*, vol. 21, no. 6, 1929.

[12] NuScale power LLC, "Passive safety Systems," [Online]. Available: http://www.nuscalepower.com/smr-benefits/safe/reactor-modules. [Accessed 26 October 2016].

[13] K. S.J, "Turbulent film condensation of high pressure steam in a vertical tube of passive secondary condensation system.," 2000.

[14] S. T. R. Seungmin Oh, "Experimental and theoretical investigation of film condensation with noncondensable gas," *International Journal of Heat and Mass Transfer,* pp. 2523-2534, 2006.

[15] K. Vierow, "Behavior of steam–air systems condensing," 1990..

[16] M. Siddique, "The effects of noncondensable gases on," 1992.

[17] V. S. ,. P. P. S.Z.Kuhn, "An investigation of condensation from steam–gas mixtures flowing downward in a vertical tube," *Nuclear Engineering and Design,* pp. 53-69, 1997.

[18] L. &. Kim, "Experimental and empirical study of steam condensation heat transfer with a noncondensable gas in a small-diameter vertical tube," 2007.

[19] J. Huang, J. Zhang and L. Wang, "Review of vapor condensation heat and mass transfer in the presence of non-condensable gas," *Applied Thermal Engineering,* no. 89, pp. 469-484, 2015.

[20] D. Ogg, "Vertical downflow condensation heat transfer in gas-steam mixtures," Berkeley, 1991.

[21] S. Kuhn, "Investigation of Heat Transfer from Condensing Steam–gas Mixtures and Turbulent Films Flowing Downward Inside a Vertical Tube," University of California, Berkeley, 1995.

[22] S. Oh and S. T. Revankar, "Boundary layer analysis for steam condensation in a vertical tube with noncondensable gases," *International Journal of Heat Exchangers,* no. 6, pp. 93-124, 2005.

[23] J.-D. Li, "CFD simulation of water vapour condensation in the presence of non-condensable gas in vertical cylindrical condensers," *International Journal of Heat and Mass Transfer,* vol. 57, no. 2, pp. 708-721, 2013.

[24] G. Zschaeck, T. Frank and A. Burns, "CFD modelling and validation of wall condensation in the presence of non-condensable gases," *Nuclear Engineering and Design,* vol. 279, pp. 137-146, 2014.

[25] W. Fu, X. Li, X. Wu and M. L. Corradini, "Numerical investigation of convective condensation with the presence of non-condensable gases in a vertical tube," *Nuclear Engineering and Design*, no. 297, pp. 197-207, 2016.

[26] K. S. V. Vierow, "Condensation in a natural circulation loop with noncondensable gases," in *Proceedings of the International Conference on Multiphase Flow*, Tsukuba, Japan, 1991.

[27] Siemens Product Lifecycle Management Software Inc, "Modeling fluid film," [Online]. Available: https://stevedocs.cd-adapco.com/starccmplus_latest_en/index.html##page/STARCCMP%2FGUID-F74F7E33-2DAC-4958-90A2-E01F9E68F34D%3Den%3D.html. [Accessed 07 January 2017].

[28] Siemens Product Lifecycle Management Software Inc, "evaporation and condensation," [Online]. Available: https://stevedocs.cd-adapco.com/starccmplus_latest_en/index.html#page/STARCCMP/GUID-265421AA-B77F-4567-BA6E-E9FE54D3104E=en=.html#wwID0EHGXVB. [Accessed 06 January 2017].

[29] Siemens Product Lifecycle Management Software Inc., "Evaporation and Condensation Solution Procedure," [Online]. Available: https://stevedocs.cd-adapco.com/starccmplus_latest_en/index.html?param=2TtEn#page/STARCCMP%2FGUID-880DC9F2-85AB-4C2A-BE6B-AD9EBE853271%3Den%3D.html. [Accessed 09 January 2017].

[30] Idaho national Laboraory, "RELAP5-3D," [Online]. Available: http://www4vip.inl.gov/relap5/default.htm.

[31] The RELAP5-3D© Code Development Team, RELAP5-3D© CODE MANUAL VOLUME IV: MODELS AND CORRELATIONS, Idaho Falls, Idaho: Idaho National Laboratory, 2014.

[32] W. Nusselt, "Die Oberflachenkondensation des Waserdampfes," *Z VDI*, vol. 60, 1916.

[33] M. M. Shah, "A General Correlation for Heat Transfer during Film Condensation Inside Pipes," *International Journal of Heat and Mass Transfer*, no. 22, pp. 547-556, 1979.

[34] W. C. Kays, Convective Heat and Mass Transfer, New York: McGraw-Hill, 1993.

[35] "NRC Westinghouse SMR," Westinghouse, [Online]. Available: http://www.nrc.gov/reactors/advanced/smr.html.

VITA

Varun Kalra was born in Uttar Pradesh, India. He was awarded his Bachelor of Engineering degree with Mechanical Engineering major, from Manipal Institute of Technology, Manipal, Karnataka, India. He initiated his Master's degree program in Nuclear Engineering major at Missouri University of Science and technology in August 2014. During his studies, he worked as a research assistant under the guidance of his advisor Dr. Joshua Schlegel. He was also awarded graduate certificate in Energy Conversion and Transport from Missouri S&T in December 2016. Finally, he was awarded a Master of Science degree in Nuclear Engineering in May 2017 from Missouri University of Science and Technology, Rolla, Missouri, USA.